CASE FILE
COPY

NACA TN 2588

NATIONAL ADVISORY COMMITTEE FOR AERONAUTICS

TECHNICAL NOTE 2588

TRANSONIC FLOW PAST A WEDGE PROFILE WITH DETACHED BOW WAVE - DETAILS OF ANALYSIS

By Walter G. Vincenti and
Cleo B. Wagoner

Ames Aeronautical Laboratory
Moffett Field, Calif.

Washington

December 1951

NATIONAL ADVISORY COMMITTEE FOR AERONAUTICS

TECHNICAL NOTE 2588

TRANSONIC FLOW PAST A WEDGE PROFILE WITH DETACHED BOW WAVE - DETAILS OF ANALYSIS

By Walter G. Vincenti and
Cleo B. Wagoner

SUMMARY

Details are given of calculations of the flow with detached bow wave past a doubly symmetrical, double-wedge profile at zero angle of attack. The results of these calculations have been described previously in NACA TN 2339. The mixed flow over the front of the profile is determined by the solution of a boundary-value problem for the transonic small-disturbance equation in the hodograph plane. The solution is obtained by the use of finite-difference equations and relaxation techniques. The methods follow established lines except for the somewhat novel treatment of the boundary conditions along the shock polar and sonic line. The purely supersonic flow over the rear of the profile is determined by means of the method of characteristics specialized to the transonic small-disturbance theory.

INTRODUCTION

The present report is the second of two NACA publications on a theoretical study of the transonic flow past a wedge profile with detached bow wave. The specific problem under consideration is that of a thin, finite wedge at zero angle of attack, with particular application to the case of the doubly symmetrical, double-wedge profile. The first report (reference 1) contains a nonmathematical outline of the general analytical method and a discussion of the final calculated

results. The present report supplements the previous work by supplying the details of the analysis.[1]

The plan of the report is briefly as follows: In the first section, the basic problem of the finite wedge with detached bow wave is stated as a boundary-value problem for the transonic small-disturbance equation in the hodograph plane. Except for the introduction of a boundary condition along the sonic line to replace conditions previously prescribed in the supersonic portion of the hodograph, this material follows the lines established by Frankl (reference 4) and Guderley (reference 5). It is recounted here primarily for the sake of completeness. In the second section of the report, the boundary-value problem in the hodograph is reduced to a system of finite-difference equations the solution of which is then obtained by relaxation techniques. This portion of the work, which constitutes the main contribution of the present report, is discussed in some detail, since it is anticipated that the methods and equations which are presented will be useful in the solution of other problems involving detached shock waves. The third section of the report describes the transformation of the hodograph solution for the finite wedge back into the physical plane. The fourth section is concerned with the characteristics construction used to obtain the purely supersonic flow over the rear of the double-wedge profile, and the final section contains a few remarks on the accuracy of the solution. It will be presumed that the reader is familiar with the general discussion of the investigation given in reference 1 or with the description of the finite-wedge problem available in reference 5, 6, or 7.[2]

---

[1]As explained in the introduction to reference 1, it was originally intended that a third report be included under the present general title. This report, written by Arthur E. Bryson, Jr., was to describe an experimental study of wedge profiles conducted at the California Institute of Technology. Because of a broadening of the experimental work to include biconvex profiles and subsonic as well as supersonic flight speeds, it now seems advisable to depart from the original plan. Bryson's report is therefore being issued by the NACA under a less restrictive title (reference 2). Certain of the results of both the theoretical and experimental studies have been given in preliminary form by Liepmann and Bryson in reference 3.

[2]The authors are indebted to William A. Mersman of the Ames Laboratory for suggestions leading to certain of the mathematical procedures used in the analysis.

NOTATION

Primary Symbols

a_*	critical speed (i.e., speed at which the speed of flow and the speed of sound are equal)
c	airfoil chord
e,f,h,k	length of irregular lattice intervals relative to that of the basic interval
$F(\lambda),G(\lambda)$	functions defined along sonic line in hodograph (See equation (6).)
I_w	integral defined by equation (39)
J_i	(i = 1, 2, 3) component integrals (See equation (33) et seq.)
K,L	functions of e, f, and $\tilde{\eta}_o$ (See equation (27).)
k_1,k_2	constants (See equations (7) and (15).)
M	Mach number
$S(\tilde{\eta})$	function defined by equation (24)
t	airfoil thickness
V	local speed of flow
x,y	Cartesian coordinates
$\tilde{Y}$	ordinate function (See page 31.)
β	absolute value of $\tilde{\eta}$ at left-hand limit of lattice
γ	ratio of specific heats (1.4 for air)
Δ	basic lattice interval
η	hodograph variable defined by equation (1)
θ	local inclination of flow

θ' variable of integration (See equation (8).)

θ_w semiangle of wedge

$\tilde{\Theta}_u, \tilde{\Theta}_d$ ordinates of upgoing and downgoing characteristics at $\tilde{\eta} = 0$ (See page 37.)

λ hodograph variable (See equation (6).)

λ' variable of integration (See equation (6).)

ξ speed parameter (See equation (49).)

ξ_o transonic similarity parameter (See equation (17).)

ρ fluid density

ψ stream function

ψ_E value of ψ at the point E (See equation (16).)

Subscripts

o conditions in free stream

o,1,2,etc. value at a prescribed lattice point

* conditions at critical speed

Superscript

$\sim$ quantity in normalized form (See equation (9).)

STATEMENT OF BOUNDARY-VALUE PROBLEM IN HODOGRAPH PLANE

Complete Hodograph

A qualitative representation of the flow over a double-wedge profile with detached bow wave is given in the first of the accompanying sketches, which differs only in detail from a similar sketch presented in reference 1. A description of this flow field is to be found in the

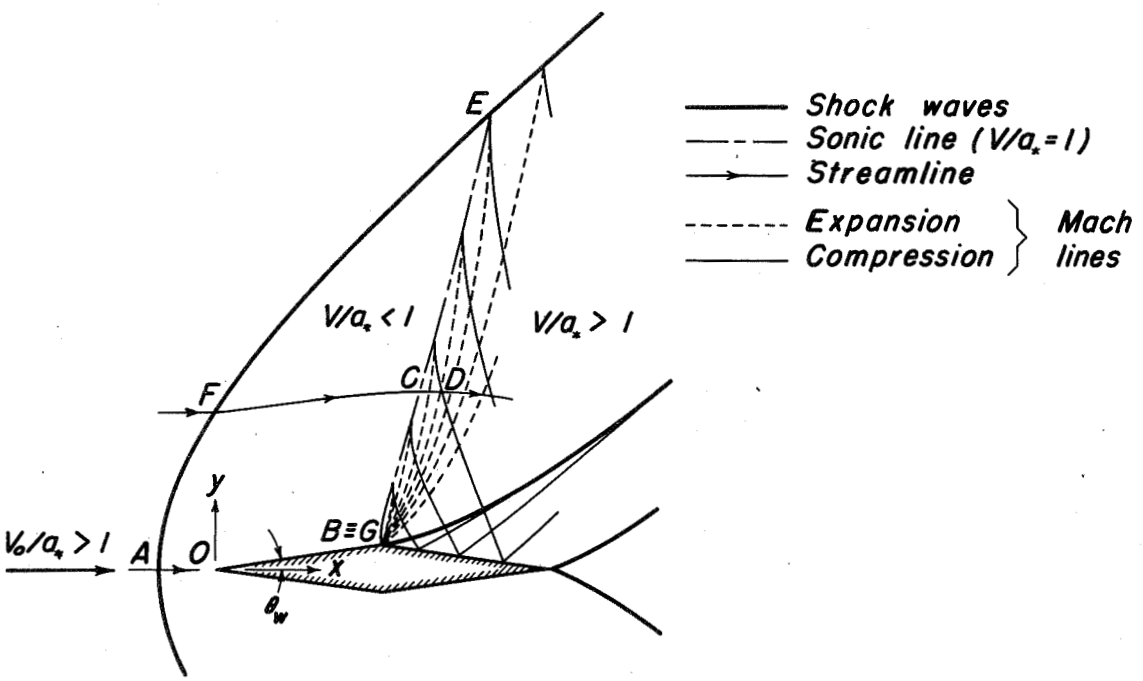

earlier paper. The second sketch shows the corresponding picture for the flow about the front half of the profile in the hodograph plane -

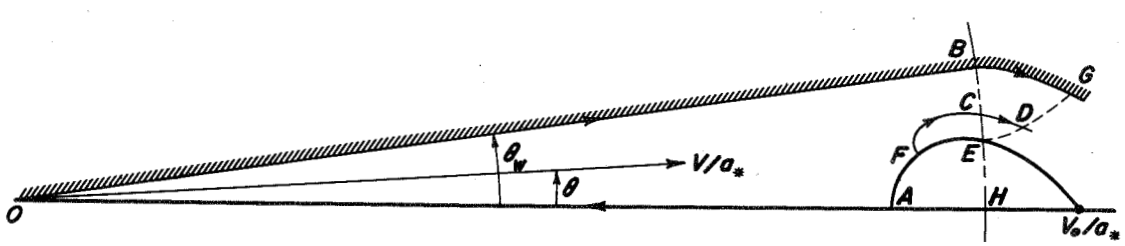

that is, in the plane V/a_*, θ where V is the local speed of flow, a_* is the critical speed, and θ is the local inclination of flow relative to the x axis.

The picture in the upper half of the hodograph plane can be described briefly as follows: The part of the shock wave which borders

upon the subsonic region in the physical plane appears in the hodograph as the subsonic portion AE of a shock polar. The shape and position of the shock polar are determined by the dimensionless free-stream velocity V_O/a_* (or, what is equivalent, by the free-stream Mach number M_O) and by the ratio of specific heats γ.[3] The portion of the central streamline from the normal part of the shock wave to the stagnation point at the nose of the wedge maps into the portion AO of the horizontal axis in the hodograph. The image of the wedge itself is given by a radial line inclined at the wedge angle θ_w and extending from the origin O to the point B on the critical circle ($V/a_* = 1$). The shoulder of the wedge, which produces an expansion fan of a locally Prandtl-Meyer type in the physical plane, appears in the hodograph as a portion of the downgoing characteristic (epicycloid) starting at B. The last Mach line from the shoulder to the sonic line (termed the separating Mach line in reference 1) appears as part of the upgoing characteristic which begins at the intersection E of the shock polar and critical circle. Point G, the point of intersection of the epicycloids from B and E, fixes the extent of the downgoing characteristic which must be considered in determining the solution in the hodograph. A typical streamline in the hodograph plane is shown by the line FCD.

To obtain a solution for the detached-wave problem in the hodograph, a boundary-value problem for the differential equations of gas dynamics must be solved within the region AOBGEA. If the stream function ψ is taken as the unknown, the pertinent boundary conditions are as follows:

1. The value of ψ is constant along the basic streamline AOBG.
2. The streamlines (i.e., the lines of constant ψ) leave the shock polar with a direction which is a known function of location on the polar.
3. The increment in ψ over the portion AE of the shock polar has a prescribed value different from zero.

The reason for the first condition is obvious. The second condition is a consequence of the requirement that, at every point on the shock polar, the direction of the shock wave as computed from the solution for ψ must be compatible with the direction given by the equations for an oblique shock wave in a uniform stream. The third condition prevents ψ from being simply a constant throughout the hodograph and, in effect, fixes the scale of the flow field in the physical plane. It will be noted that no condition is prescribed along the boundary EG in the hodograph. Frankl has proved (reference 4) that the solution determined by the foregoing boundary conditions is unique.

---

[3]The equations which are pertinent here can be found in the work of Frankl (reference 4).

Specialization to Small Disturbances

Original boundary-value problem.- As has been shown by Guderley (reference 5), the equations of the boundary-value problem in the hodograph are considerably simplified when restriction is made to the neighborhood of the critical speed. To this end, the quantity η is introduced according to the relation

$$\eta = (\gamma+1)^{1/3} \frac{V-a_*}{a_*} \tag{1}$$

and η and the stream angle θ are assumed sufficiently small that only their lowest powers need be retained in the analysis. This means, in effect, that the right-hand portion of the previous hodograph (including the shock polar itself) is made to shrink down to the vicinity of the point H, which defines the intersection of the critical circle and the horizontal axis.

When the foregoing procedure is carried out and the limiting process is counteracted by a suitable enlargement of scale, the situation in the small-disturbance hodograph (i.e., in the η,θ plane) appears as in the adjacent sketch. Here the critical speed corresponds

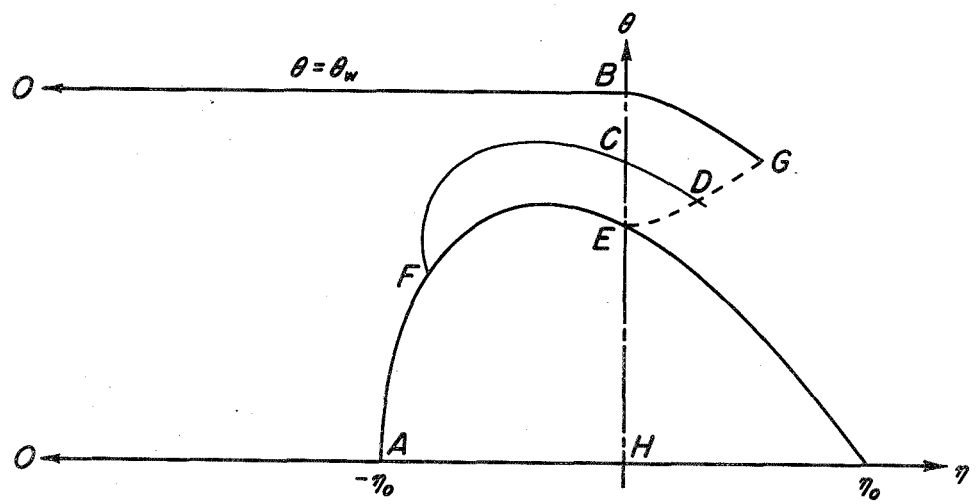

to the vertical axis $\eta = 0$. The equation for the upper half of the shock polar in the simplified hodograph has the form

$$\theta = (\eta_0-\eta)\sqrt{\frac{\eta_0+\eta}{2}} \tag{2}$$

where η_o is the value of η corresponding to the free-stream velocity V_o.[4] By virtue of the limiting process, the stagnation point at O has moved, in the present system of axes, infinitely far to the left. As a result, the part AO of the horizontal axis ($\theta = 0$) extends now from $\eta = -\eta_o$ to $\eta = -\infty$. The image OB of the wedge is similarly represented by the horizontal line $\theta = \theta_w$, $\eta \leqq 0$. The characteristics, which complete the boundaries of the field, have the simple form

$$\theta = \text{const.} \pm \frac{2}{3} \eta^{3/2} \tag{3}$$

On the basis of the usual assumptions regarding flow near the critical speed, the differential equation for ψ reduces, in the present simplified hodograph, to the form

$$\psi_{\eta\eta} - \eta\psi_{\theta\theta} = 0 \tag{4}$$

This is the mixed elliptic-hyperbolic equation studied by Tricomi in reference 8. The boundary conditions along the central streamline require that ψ is constant - say 0 - on AO and OBG and that $\psi \to 0$ as $\eta \to (-\infty)$ for $0 \leqq \theta \leqq \theta_w$. On the upper half of the shock polar, the boundary conditions require that the lines of constant ψ must have the slope

$$\frac{d\theta}{d\eta} = -\frac{\eta_o+7\eta}{3\eta_o+5\eta}\sqrt{\frac{\eta_o+\eta}{2}} \tag{5a}$$

On a line of constant ψ, $d\theta/d\eta$ can be replaced by $-\psi_\eta/\psi_\theta$, so that the foregoing condition can also be written

$$\psi_\eta - \frac{\eta_o+7\eta}{3\eta_o+5\eta}\sqrt{\frac{\eta_o+\eta}{2}}\,\psi_\theta = 0 \tag{5b}$$

The final boundary condition requires that ψ must have some given value $\psi_E (\neq 0)$ at the point E. Since the coordinates of the flow field will ultimately be expressed in terms of a characteristic dimension of the wedge, the actual value assigned to ψ_E is purely a matter of convenience. As before, no boundary condition is specified along the characteristic EG.

---

[4] The derivation of this and the other equations for the simplified hodograph is given by Guderley in reference 5.

Elimination of the supersonic region.- The foregoing is the boundary-value problem for the finite wedge as formulated by Guderley. It was the original intention in the present work to obtain a numerical solution of this problem on the basis of the boundaries and boundary conditions which have been described. Efforts in this direction failed, however, because of difficulties in obtaining convergence of the relaxation process in the supersonic portion BGE of the hodograph.[5] Similar difficulties have been reported in references 9 and 10 with regard to relaxation calculations of the transonic flow through a converging-diverging nozzle. The reasons for the difficulty in the present case are not apparent. Fundamental questions would appear to be involved concerning the stability and convergence of the finite-difference scheme for the Tricomi equation in the hyperbolic domain. A study of these matters, similar perhaps to that reported for the wave equation in reference 11, may be a prerequisite to numerical solutions of mixed-flow problems in the general case. In the present example, however, the difficulty can be circumvented by modifying the boundary-value problem so as to eliminate the supersonic region from explicit consideration.

The elimination of the supersonic region depends on a formula given by Tricomi (reference 8, equation (2.19)) which relates the behavior of ψ on the vertical axis to its behavior on a characteristic. In the present case, in which ψ is identically zero on the characteristic BG, this formula reduces to an integral relation between ψ and ψ_η at points on the sonic line. This relation has the form

$$F(\lambda) = -k_1 \int_0^\lambda \frac{G(\lambda')}{(\lambda-\lambda')^{1/3}}\, d\lambda' \tag{6}$$

where

$$\lambda = \theta_w - \theta$$

$$F(\lambda) = \psi(0,\theta)$$

$$G(\lambda) = \psi_\eta(0,\theta)$$

and λ' is a variable of integration. (See sketch.)

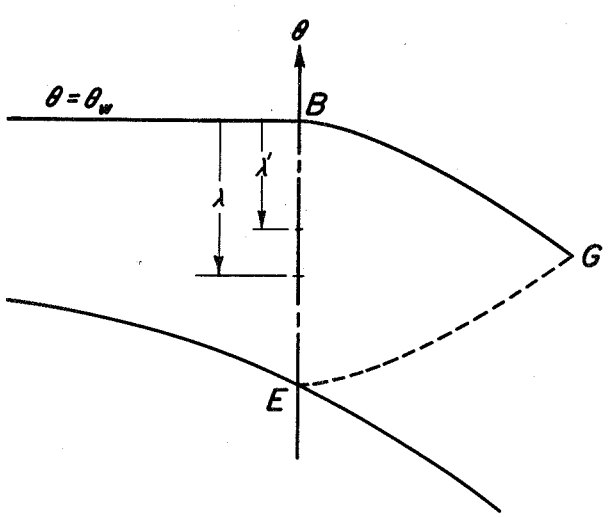

[5]Several procedures were tried in the supersonic region, using both a square lattice and a lattice following the characteristics. All were unsuccessful.

The numerical constant k_1 is given by

$$k_1 = \frac{3^{2/3}\,\Gamma^3(1/3)}{4\pi^2} \tag{7a}$$

where $\Gamma(1/3)$ is the gamma function of the argument $1/3$. For the accuracy required in the later numerical work, the value of this constant may be taken as

$$k_1 = 1.013 \tag{7b}$$

Satisfying equation (6) everywhere on the sonic line from B to E is completely equivalent to satisfying the condition $\psi = 0$ on the downgoing characteristic from B to G.

For the present application, it is convenient to invert equation (6), which can be done by means of Abel's formula. This gives (see reference 12, p. 229)

$$G(\lambda) = -\frac{\sqrt{3}}{2\pi k_1}\frac{d}{d\lambda}\int_0^\lambda \frac{F(\lambda')}{(\lambda-\lambda')^{2/3}}\,d\lambda'$$

The differentiation indicated on the right is readily accomplished by first transforming the integral to one with fixed limits by means of the substitution $\lambda' = t\lambda$. The result is, after reverting to the original notation,

$$G(\lambda) = -\frac{\sqrt{3}}{2\pi k_1}\frac{1}{\lambda}\left[\frac{1}{3}\int_0^\lambda \frac{F(\lambda')}{(\lambda-\lambda')^{2/3}}\,d\lambda' + \int_0^\lambda \frac{\lambda' F_\lambda(\lambda')}{(\lambda-\lambda')^{2/3}}\,d\lambda'\right]$$

Transforming the first integral through integration by parts and noting that $F(0) = 0$, one obtains finally

$$G(\lambda) = -\frac{\sqrt{3}}{2\pi k_1}\int_0^\lambda \frac{F_\lambda(\lambda')}{(\lambda-\lambda')^{2/3}}\,d\lambda'$$

This can be written in the η,θ notation as

$$\psi_\eta(0,\theta) + \frac{\sqrt{3}}{2\pi k_1} \int_{\theta_w}^{\theta} \frac{\psi_\theta(0,\theta')}{(\theta'-\theta)^{2/3}}\, d\theta' = 0 \tag{8}$$

where $\theta' = \theta_w - \lambda'$ denotes the variable of integration. As with equation (6), satisfaction of equation (8) everywhere on the sonic line between B and E insures that ψ is zero everywhere on the characteristic from B to G. By regarding equation (8) as a boundary condition along BE, the region of solution of the partial differential equation (4) can be confined to the purely subsonic portion of the hodograph ($\eta \leqq 0$). Relaxation methods can be used to solve the resulting elliptic problem without essential difficulty.

Equations in normalized form.- To carry out the numerical calculations, it is convenient to normalize the equations of the boundary-value problem by means of the transformation

$$\tilde{\eta} = \frac{\eta}{\eta_o}, \qquad \tilde{\theta} = \sqrt{2}\,\frac{\theta}{\eta_o^{3/2}} \tag{9}$$

This is equivalent to introducing the rules for transonic similarity. (See, for example, references 5, 13, and 14.) The particular form of transformation chosen here has the advantage for the present work of providing a unique shock polar with conveniently located horizontal and vertical intercepts.

With the foregoing substitution, the differential equation (4) takes on the following form in the $\tilde{\eta},\tilde{\theta}$ plane:

$$\psi_{\tilde{\eta}\tilde{\eta}} - 2\tilde{\eta}\,\psi_{\tilde{\theta}\tilde{\theta}} = 0 \tag{10}$$

Consistent with the elimination of the supersonic region, the boundary-value problem can now be summarized as follows (see sketch):

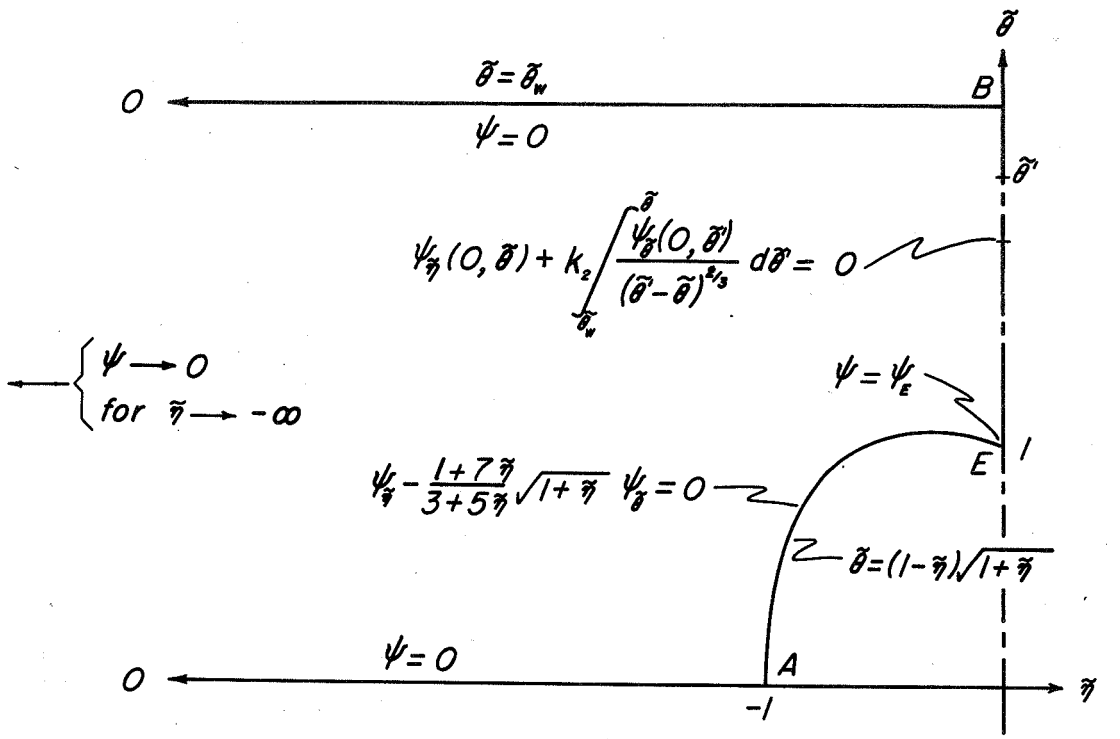

1. On the basic streamline AOB:

$$\psi = 0 \text{ for } \tilde{\theta} = 0,\ \tilde{\eta} \leqq -1 \tag{11}$$

$$\psi = 0 \text{ for } \tilde{\theta} = \tilde{\theta}_w,\ \tilde{\eta} \leqq 0 \tag{12}$$

$$\psi \to 0 \text{ for } \tilde{\eta} \to -\infty,\ 0 \leqq \tilde{\theta} \leqq \tilde{\theta}_w \tag{13}$$

2. On the shock polar AE:

$$\psi_{\tilde{\eta}} - \frac{1+7\tilde{\eta}}{3+5\tilde{\eta}}\sqrt{1+\tilde{\eta}}\,\psi_{\tilde{\theta}} = 0$$

for

$$\tilde{\theta} = (1-\tilde{\eta})\sqrt{1+\tilde{\eta}},\ -1 \leqq \tilde{\eta} \leqq 0 \tag{14}$$

3. On the sonic line BE:

$$\psi_{\tilde{\eta}}(0,\tilde{\theta}) + k_2 \int_{\tilde{\theta}_w}^{\tilde{\theta}} \frac{\psi_{\tilde{\theta}}(0,\tilde{\theta}')}{(\tilde{\theta}'-\tilde{\theta})^{2/3}}\, d\tilde{\theta}' = 0$$

for

$$1 \leqq \tilde{\theta} \leqq \tilde{\theta}_w$$

where

$$k_2 = \frac{3^{1/2}}{2^{2/3}\pi k_1} \tag{15}$$

4. At the point E:

$$\psi = \psi_E \text{ (arbitrary constant } \neq 0) \text{ for } \tilde{\eta} = 0,\ \tilde{\theta} = 1 \tag{16}$$

It is apparent from the preceding equations that a solution of the problem will depend on only the single parameter $\tilde{\theta}_w$, which defines the position of the upper boundary in the $\tilde{\eta},\tilde{\theta}$ plane. This parameter is directly related to the more familiar transonic similarity parameter

$$\xi_0 \cong \frac{M_0^2-1}{[(\gamma+1)(t/c)]^{2/3}} \tag{17}$$

which was used as a basis for the presentation of the results in reference 1. (In this equation, t/c is the thickness ratio of the double-wedge profile. It is equal, to the present order of accuracy, to the wedge angle θ_w.) The relation between ξ_0 and $\tilde{\theta}_w$, easily derived from equations (1) and (9) of the present paper and equation (21) of reference 1, is given by

$$\xi_0 = \frac{2^{1/3}}{\tilde{\theta}_w^{2/3}} \tag{18}$$

SOLUTION OF BOUNDARY-VALUE PROBLEM IN HODOGRAPH PLANE

The solution of the boundary-value problem in the $\tilde{\eta},\tilde{\theta}$ plane is obtained in two steps, according to established procedures for the numerical treatment of partial differential equations. (For introductory articles, see references 15, 16, and 17. For an extended discussion, see reference 18.) In the first step, the domain under

consideration is covered by a square lattice, and a finite-difference approximation to the differential equation or boundary condition is written for each lattice point. The boundary-value problem for the partial differential equation is thus reduced to a problem in solving a large number of simultaneous algebraic equations. Solution of the latter problem by relaxation methods is the second step.

Reduction to Finite-Difference Equations

The arrangement of a typical finite-difference lattice in the $\tilde{\eta},\tilde{\theta}$ plane is shown in figure 1. The basic lattice interval, which is the same in both directions, is denoted by Δ. Adjacent to the shock polar, the interval is adjusted so that the terminal lattice points lie on the polar itself. For purposes of formulating the finite-difference equations, the lattice points are conveniently grouped into five categories as follows (typical points in each category are indicated in the figure):

a. Regular internal points
b. Points far to the left
c. Points adjacent to the shock polar
d. Points on the shock polar
e. Points on the sonic line

The form of the finite-difference equation pertinent to each category will be developed in the subsequent paragraphs. The methods employed are standard, except for the somewhat novel treatment of the boundary conditions along the shock polar and sonic line.

Regular internal points.- The category of regular internal points comprises all points interior to the boundaries but not immediately adjacent to the shock polar. The situation in the vicinity of such a point is as shown in the sketch. The difference equation which applies here is obtained by suitable approximation to the differential equation (10).

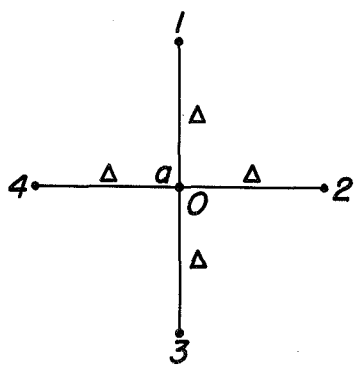

If it is assumed that the unknown function $\psi = \psi(\tilde{\eta},\tilde{\theta})$ may be expanded locally in the form of a Taylor's series, the values of ψ at 2 and 4 may be written (see sketch)

$$\psi_2 = \psi_0 + \Delta \psi_{\tilde{\eta}}\Big|_0 + \frac{\Delta^2}{2!} \psi_{\tilde{\eta}\tilde{\eta}}\Big|_0 + \frac{\Delta^3}{3!} \psi_{\tilde{\eta}\tilde{\eta}\tilde{\eta}}\Big|_0 + O(\Delta^4)$$

$$\psi_4 = \psi_0 - \Delta \psi_{\tilde{\eta}}\Big|_0 + \frac{\Delta^2}{2!} \psi_{\tilde{\eta}\tilde{\eta}}\Big|_0 - \frac{\Delta^3}{3!} \psi_{\tilde{\eta}\tilde{\eta}\tilde{\eta}}\Big|_0 + O(\Delta^4)$$

Addition of these equations and solution for $\psi_{\tilde{\eta}\tilde{\eta}}\Big|_0$ gives

$$\psi_{\tilde{\eta}\tilde{\eta}}\Big|_0 = \frac{1}{\Delta^2} (\psi_4 - 2\psi_0 + \psi_2) + O(\Delta^2) \tag{19a}$$

which is a well-known difference expression for the second derivative. The corresponding derivative in the vertical direction is similarly represented by

$$\psi_{\tilde{\theta}\tilde{\theta}}\Big|_0 = \frac{1}{\Delta^2} (\psi_3 - 2\psi_0 + \psi_1) + O(\Delta^2) \tag{19b}$$

Substituting these expressions into the differential equation (10) and neglecting the terms of $O(\Delta^2)$ then gives for the finite-difference equation at a regular internal point

$$\psi_2 + \psi_4 - 2\tilde{\eta}_0(\psi_1 + \psi_3) - 2(1 - 2\tilde{\eta}_0)\psi_0 = 0 \tag{20}$$

where $\tilde{\eta}_0$ denotes the horizontal coordinate of the point in question. The difference equation for internal points is thus the same for points on a given column but differs from one column to the next. For a point adjacent to the upper boundary OB — as, for example, the point a' in figure 1 — the value of ψ_1 must be set equal to zero in accord with the boundary condition (12). Similar considerations hold for points adjacent to the lower boundary OA.

Equation (20) represents the simplest possible finite-difference approximation to the differential equation (10). As is apparent from the derivation, the error involved is of $O(\Delta^2)$. Consideration has been given to improving the approximation by including additional lattice points in the finite-difference equation or by incorporating higher-order difference corrections in the later relaxation work (cf., references 19, 20, and 21). Because of the complicated nature of the boundary conditions along the shock polar and sonic line, however, consistent application of these procedures did not appear feasible. The requisite accuracy in the present work has therefore been achieved by suitable decrease in the mesh interval Δ in those regions in which

the function ψ varies most rapidly. This procedure has the secondary advantage of providing closely spaced values of the derivatives which are required for the later transformation to the physical plane.

Points far to the left.- In order to carry through the numerical analysis, it is necessary that the finite-difference lattice be terminated at some distance to the left in the hodograph. This can be done with the aid of an asymptotic solution valid for large negative values of $\tilde{\eta}$.

By separation of variables, it can be shown that the general solution of the differential equation (10) in the region $\tilde{\eta} \leq -1$, $0 \leq \tilde{\theta} \leq \tilde{\theta}_w$, subject to the boundary conditions (11), (12), and (13), is

$$\psi = \sum_{n=1}^{\infty} A_n \sqrt{-\tilde{\eta}} \sin\left(\frac{n\pi\tilde{\theta}}{\tilde{\theta}_w}\right) K_{1/3}\left[\frac{n\pi}{3\tilde{\theta}_w}(-2\tilde{\eta})^{3/2}\right]$$

where $K_{1/3}$ is the modified Bessel function of the second kind of order 1/3 (notation of reference 22) and A_n is an appropriate constant. At sufficiently large negative values of $\tilde{\eta}$ the first term of the series will predominate, and the above solution can be approximated by

$$\psi = A \sqrt{-\tilde{\eta}} \sin\left(\frac{\pi\tilde{\theta}}{\tilde{\theta}_w}\right) K_{1/3}\left[\frac{\pi}{3\tilde{\theta}_w}(-2\tilde{\eta})^{3/2}\right]$$

If $K_{1/3}$ is then replaced by the first term of its asymptotic expansion (reference 22, p. 202)

$$K_{1/3}(z) \cong \sqrt{\frac{\pi}{2z}}\, e^{-z}$$

there results finally for ψ the expression

$$\psi = B \sin\left(\frac{\pi\tilde{\theta}}{\tilde{\theta}_w}\right) \times (-\tilde{\eta})^{-1/4} \exp\left[-\frac{\pi}{3\tilde{\theta}_w}(-2\tilde{\eta})^{3/2}\right] \qquad (21)$$

where B is an unknown constant.

The asymptotic solution (21) makes it possible to terminate the finite-difference lattice at a position on the left. Consider a typical lattice point in a column located at $\tilde{\eta}=-\beta$ (as, for example, the

point b in fig. 1). The neighboring points are then as shown in the adjacent sketch, where the point 4 now represents a ficticious lattice point located at $\tilde{\eta} = -(\beta+\Delta)$. If β is taken sufficiently large that $\Delta/\beta << 1$, then it follows from equation (21) that, to a first order of approximation,

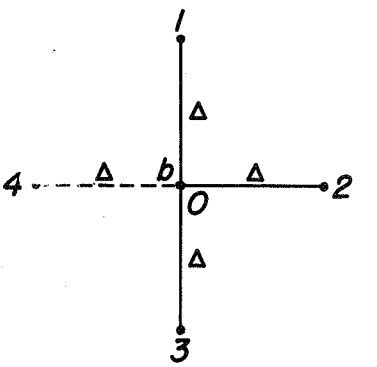

$$\frac{\psi_4}{\psi_0} = \left(1 - \frac{\Delta}{4\beta}\right) \exp\left(-\frac{\pi\Delta}{\tilde{\theta}_w}\sqrt{2\beta}\right)$$

Substitution of this value of ψ_4 into the previous equation (20) gives for the finite-difference equation at a point on the left-hand boundary

$$\psi_2 + 2\beta(\psi_1+\psi_3) + \left[\left(1 - \frac{\Delta}{4\beta}\right) \exp\left(-\frac{\pi\Delta}{\tilde{\theta}_w}\sqrt{2\beta}\right) - 2(1+2\beta)\right]\psi_0 = 0 \qquad (22)$$

The value of β to be used in any particular case is determined on the basis of computational experience. In general, the larger the value of $\tilde{\theta}_w$, the larger must be the value of β to assure that the use of the asymptotic solution (21) is justified. Since the over-all result is insensitive to changes in the left-hand portion of the field, however, the choice of β is not a critical matter.

Points adjacent to the shock polar.- Points adjacent to the shock polar require special treatment because of the irregularity of the intervals encountered near the curved boundary. Consider the typical case shown in the sketch (corresponding to point c in fig. 1). Here h and k define the length of the irregular intervals relative to that of the regular interval Δ.

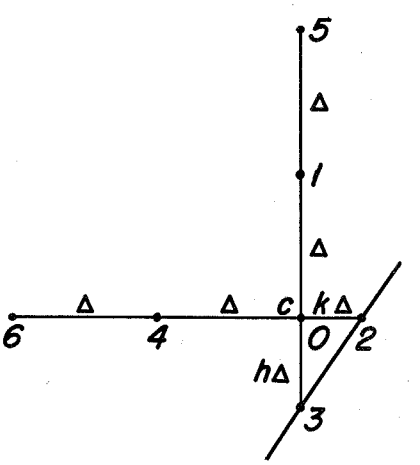

To obtain the desired accuracy, it was found advisable in the present case to include three rather than two neighboring points in each of the coordinate directions. The value of ψ at the points 2, 4, and 6 is therefore written

$$\psi_2 = \psi_0 + k\Delta \psi_{\tilde{\eta}}\Big|_0 + \frac{(k\Delta)^2}{2!} \psi_{\tilde{\eta}\tilde{\eta}}\Big|_0 + \frac{(k\Delta)^3}{3!} \psi_{\tilde{\eta}\tilde{\eta}\tilde{\eta}}\Big|_0 + O(\Delta^4)$$

$$\psi_4 = \psi_0 - \Delta \psi_{\tilde{\eta}}\Big|_0 + \frac{\Delta^2}{2!} \psi_{\tilde{\eta}\tilde{\eta}}\Big|_0 - \frac{\Delta^3}{3!} \psi_{\tilde{\eta}\tilde{\eta}\tilde{\eta}}\Big|_0 + O(\Delta^4)$$

$$\psi_6 = \psi_0 - 2\Delta \psi_{\tilde{\eta}}\Big|_0 + \frac{(2\Delta)^2}{2!} \psi_{\tilde{\eta}\tilde{\eta}}\Big|_0 - \frac{(2\Delta)^3}{3!} \psi_{\tilde{\eta}\tilde{\eta}\tilde{\eta}}\Big|_0 + O(\Delta^4)$$

These may be looked upon as constituting three simultaneous equations for the first three derivatives of ψ in the horizontal direction at the point 0. Solution of these equations for $\psi_{\tilde{\eta}\tilde{\eta}}\Big|_0$ gives

$$\psi_{\tilde{\eta}\tilde{\eta}}\Big|_0 = \frac{1}{\Delta^2}\left[-\frac{1-k}{2+k}\psi_6 + \frac{2(2-k)}{1+k}\psi_4 - \frac{3-k}{k}\psi_0 + \frac{6}{k(1+k)(2+k)}\psi_2\right] + O(\Delta^2)$$

The corresponding expression for $\psi_{\tilde{\theta}\tilde{\theta}}\Big|_0$ is identical except that k is replaced by h and ψ_2, ψ_4, and ψ_6 by ψ_3, ψ_1, and ψ_5, respectively. Substituting these expressions for the two second derivatives into the differential equation (10) and neglecting terms of $O(\Delta^2)$ then gives for the finite-difference equation at 0

$$\frac{6}{k(1+k)(2+k)}\psi_2 + \frac{2(2-k)}{1+k}\psi_4 - \frac{1-k}{2+k}\psi_6 - 2\tilde{\eta}_0\left[\frac{6}{h(1+h)(2+h)}\psi_3 + \frac{2(2-h)}{1+h}\psi_1 - \frac{1-h}{2+h}\psi_5\right] - \left[\frac{3-k}{k} - 2\tilde{\eta}_0\frac{3-h}{h}\right]\psi_0 = 0 \qquad (23)$$

This reduces to the previous equation (20) when $k = h = 1$. (The functions of h and k which appear here have been tabulated in reference 23. The intervals of tabulation are not always sufficiently small, however, to provide the accuracy needed in the present work.)

Points on the shock polar.- In past applications of numerical methods to problems involving curved boundaries, it has not ordinarily been the practice to use a lattice with points located on the boundary itself. The prescribed boundary conditions have then been incorporated in the following manner (cf. references 24 and 25): First, the finite-difference lattice is extended, on the basis of the regular lattice spacing, to include ficticious points external to the boundary. This makes the lattice geometry at internal points adjacent to the boundary

the same as at all regular internal points. Next, with the aid of the boundary conditions and suitable interpolation and extrapolation formulas, an expression is obtained for the independent variable at each external point in terms of the values at neighboring internal points. Finally, by substituting these expressions into the finite-difference equation for a regular point, the difference equations are written for the internal points adjacent to the boundary. In this way the boundary conditions are incorporated implicitly into the difference equations at internal points. The procedure is parallel in many respects to that used in terminating the present lattice at the left-hand side of the field.

Although a procedure of the foregoing type can be devised to take care of the boundary conditions on the shock polar, a different approach was found advantageous for the present work. In this approach, the lattice points are placed directly on the boundary as previously described, and a difference equation is obtained at each such point by suitable finite-difference approximation to the boundary condition. This leads to a somewhat larger system of simultaneous equations than would the more usual procedure but has been found in the long run to give more accurate results with less total effort.

The boundary condition (14), which is thus the basis for the finite-difference equations on the shock polar, can be written

$$\underset{\sim}{\psi}_{\eta} - S(\tilde{\eta})\, \underset{\sim}{\psi}_{\theta} = 0 \tag{24}$$

where

$$S(\tilde{\eta}) = \frac{1+7\tilde{\eta}}{3+5\tilde{\eta}} \sqrt{1+\tilde{\eta}}$$

The problem now is to determine difference expressions for the derivatives $\underset{\sim}{\psi}_{\eta}$ and $\underset{\sim}{\psi}_{\theta}$ at points on the polar. Consider, for example, the typical situation shown in the sketch (corresponding to point d of fig. 1). To determine $\underset{\sim}{\psi}_{\theta}$, the value of ψ at each of the interior points 1, 2, and 3 is written, as before, in terms of a Taylor's series about the boundary point 0. Solving the resulting three equations for the derivative $\underset{\sim}{\psi}_{\theta}$ at 0 then gives

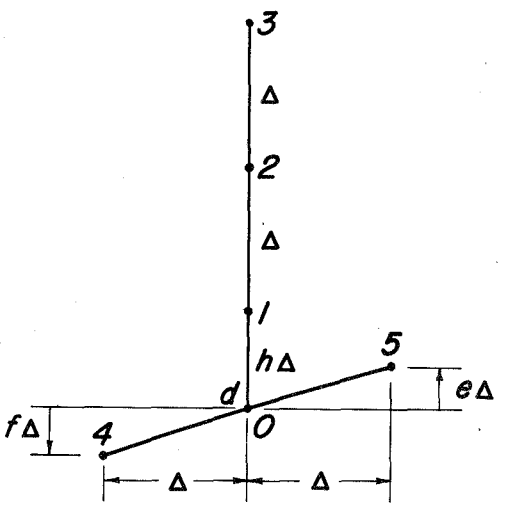

$$\psi_{\tilde{\theta}}\Big|_o = \frac{1}{\Delta}\left[-\frac{h(2+h)+2(1+h)^2}{h(1+h)(2+h)}\psi_o + \frac{(1+h)(2+h)}{2h}\psi_1 - \frac{h(2+h)}{1+h}\psi_2 + \frac{h(1+h)}{2(2+h)}\psi_3\right] + O(\Delta^3) \tag{25}$$

This expression, which includes terms of $O(\Delta^2)$, is inconsistent in order of accuracy with the expressions previously employed in setting up the finite-difference equations at internal points. Since end differentiation is, even for a given order of mathematical accuracy, inherently less precise than differentiation at a midpoint (see error terms in reference 23), the retention of the second-order terms was here thought advisable.

The determination of the corresponding expression for $\psi_{\tilde{\eta}}$ is a bit more involved. Expanding ψ at the boundary points 4 and 5 by means of a Taylor's series in two dimensions gives

$$\psi_4 = \psi_o - \Delta\,\psi_{\tilde{\eta}}\Big|_o - f\Delta\,\psi_{\tilde{\theta}}\Big|_o + \frac{\Delta^2}{2!}\psi_{\tilde{\eta}\tilde{\eta}}\Big|_o + f\Delta^2\,\psi_{\tilde{\eta}\tilde{\theta}}\Big|_o + \frac{(f\Delta)^2}{2!}\psi_{\tilde{\theta}\tilde{\theta}}\Big|_o + O(\Delta^3)$$

$$\psi_5 = \psi_o + \Delta\,\psi_{\tilde{\eta}}\Big|_o + e\Delta\,\psi_{\tilde{\theta}}\Big|_o + \frac{\Delta^2}{2!}\psi_{\tilde{\eta}\tilde{\eta}}\Big|_o + e\Delta^2\,\psi_{\tilde{\eta}\tilde{\theta}}\Big|_o + \frac{(e\Delta)^2}{2!}\psi_{\tilde{\theta}\tilde{\theta}}\Big|_o + O(\Delta^3)$$

An expression for $\psi_{\tilde{\theta}}\Big|_o$ is already known from equation (25) in terms of ψ_o, ψ_1, ψ_2, and ψ_3; and an expression for $\psi_{\tilde{\theta}\tilde{\theta}}\Big|_o$ can similarly be determined. The two foregoing expansions may thus be regarded as constituting two equations for the three unknowns $\psi_{\tilde{\eta}}\Big|_o$, $\psi_{\tilde{\eta}\tilde{\eta}}\Big|_o$, and $\psi_{\tilde{\eta}\tilde{\theta}}\Big|_o$. To solve for $\psi_{\tilde{\eta}}\Big|_o$, one more equation is necessary. This is provided by the differental equation (10), which also applies on the boundary and which may be written at the point 0 as

$$\psi_{\tilde{\eta}\tilde{\eta}\tilde{\eta}}\Big|_o - 2\tilde{\eta}_o\,\psi_{\tilde{\theta}\tilde{\theta}}\Big|_o = 0$$

The solution for $\psi_{\tilde{\eta}}\Big|_o$ is then found as

$$\psi_{\tilde{\eta}}\Big|_o = \frac{1}{\Delta}\left\{-\frac{e}{e+f}\psi_4 - \frac{e-f}{e+f}\psi_o + \frac{f}{e+f}\psi_5 - \frac{2ef}{e+f}\psi_{\tilde{\theta}}\Big|_o + \frac{1}{2}\frac{e-f}{e+f}(2\tilde{\eta}_o - ef)\right.$$

$$\left.\left[\frac{6}{h(2+h)}\psi_o - \frac{3+2h}{h}\psi_1 + 4\psi_2 - \frac{1+2h}{2+h}\psi_3\right]\right\} + O(\Delta^2) \qquad (26)$$

where $\psi_{\tilde{\theta}}\Big|_o$ is given by the previous equation (25).[6]

The required finite-difference equation for the point on the shock polar can now be obtained by substituting expressions (25) and (26) into the boundary condition (24) and neglecting the higher-order terms in each case. The result can finally be written

$$\frac{(1+h)(2+h)+2L(3+2h)}{2h}\psi_1 - \frac{h(2+h)+4L(1+h)}{1+h}\psi_2 + \frac{h(1+h)+2L(1+2h)}{2(2+h)}\psi_3 +$$

$$eK\psi_4 - fK\psi_5 - \left[\frac{h(2+h)+2(1+h)^2}{h(1+h)(2+h)} + \frac{6L}{h(2+h)} + (e-f)K\right]\psi_o = 0 \qquad (27)$$

where $K = K(e,f,\tilde{\eta}_o)$ and $L = L(e,f,\tilde{\eta}_o)$ are given by

$$K = \frac{1}{(e+f)S(\tilde{\eta}_o)+2ef}$$

$$L = (e-f)\left(\tilde{\eta}_o - \frac{ef}{2}\right)K$$

Equation (27) is convenient for points on the shock polar for which $-0.6 \leq \tilde{\eta} < 0$. For $-1 < \tilde{\eta}_o < -0.6$, the general procedure is the

---

[6]It will be noted that the coefficients in equation (26) become undesirably large as $f \rightarrow -e$ and are undefined when $f = -e$. This results from the fact that the determinant of the coefficients in the simultaneous equations used to obtain $\psi_{\tilde{\eta}}\Big|_o$ vanishes when $f = -e$. Difficulties from this source can be avoided by judicious choice of the lattice points.

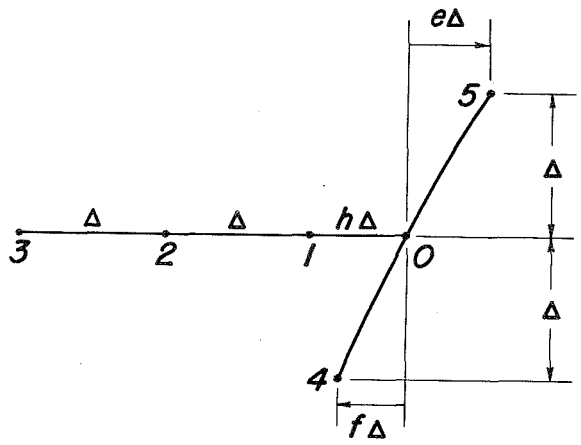

same except that the points 0, 1, 2, and 3 are now more conveniently located on a horizontal line and the quantities e, f, and h are redefined accordingly (see sketch). The resulting finite-difference equation is identical with equation (27) except that the terms which previously arose from the expression for $\psi_{\tilde{\theta}}\big|_0$ are now multiplied by -1.

Points on the sonic line.- The difference equation for points on the sonic line is obtained by finite-difference approximation to the boundary condition (15), which can be written, to the accuracy required in the numerical work, as

$$\psi_{\tilde{\eta}}(0,\tilde{\theta}) + 0.342 \int_{\tilde{\theta}_w}^{\tilde{\theta}} \frac{\psi_{\tilde{\theta}}(0,\tilde{\theta}')}{(\tilde{\theta}'-\tilde{\theta})^{2/3}}\, d\tilde{\theta}' = 0 \qquad (28)$$

The procedure varies depending on whether the difference equation is being written for the first point below the upper boundary or for one of the lower points.

First point below boundary:

At the first point below the upper boundary the situation is as indicated. To approximate the integral in equation (28), use is made of Guderley's singular solution for transonic flow over a convex corner (reference 26). On the basis of this solution, it can be shown that the variation of ψ along the vertical axis in the immediate vicinity of the point B is of the form

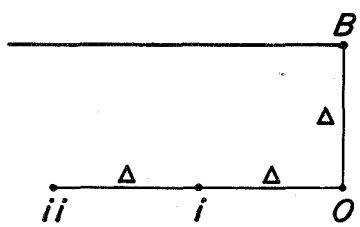

$$\psi \sim (\tilde{\theta}_w - \tilde{\theta})^{4/3} \qquad (29)$$

If the lattice spacing is made sufficiently small, this asymptotic relation may be taken as approximately correct over the entire interval from B to 0, so that within this interval

$$\psi = \psi_o \left(\frac{\tilde{\theta}_w - \tilde{\theta}}{\Delta} \right)^{4/3}$$

and

$$\psi_{\tilde{\theta}} = - \frac{4}{3} \psi_o \frac{(\tilde{\theta}_w - \tilde{\theta})^{1/3}}{\Delta^{4/3}}$$

For the first point below the boundary, the integral in equation (28) can thus be written

$$\int_{\tilde{\theta}_w}^{\tilde{\theta}} \frac{\psi_{\tilde{\theta}}(0, \tilde{\theta}')}{(\tilde{\theta}' - \tilde{\theta})^{2/3}} d\tilde{\theta}' = - \frac{4\psi_o}{3\Delta^{4/3}} \int_{\tilde{\theta}_w}^{\tilde{\theta}_w - \Delta} \frac{(\tilde{\theta}_w - \tilde{\theta}')^{1/3}}{[\Delta - (\tilde{\theta}_w - \tilde{\theta}')]^{2/3}} d\tilde{\theta}' =$$

$$\frac{4\psi_o}{3\Delta^{2/3}} \int_0^1 \frac{\tau^{1/3}}{(1-\tau)^{2/3}} d\tau$$

where $\tau = (\tilde{\theta}_w - \tilde{\theta}')/\Delta$. The integral on the right can be reduced to standard form by means of the substitution $\tau(1-\tau) = 1/4\ z^3$, which gives

$$\int_0^1 \frac{\tau^{1/3}}{(1-\tau)^{2/3}} d\tau = \frac{3}{2^{2/3}} \int_0^1 \frac{dz}{\sqrt{1-z^3}}$$

This is an elliptic integral of the first kind. Its value, as determined from the equations and tables of reference 27, is

$$\int_0^1 \frac{\tau^{1/3}}{(1-\tau)^{2/3}} d\tau = \frac{3}{2^{2/3}} \times \frac{1.846}{3^{1/4}} = 2.650$$

The integral in equation (28) thus becomes, in the present case,

$$\int_{\tilde{\theta}_w}^{\tilde{\theta}} \frac{\psi_{\tilde{\theta}}(0, \tilde{\theta}')}{(\tilde{\theta}' - \tilde{\theta})^{2/3}} d\tilde{\theta}' = \frac{4}{3} \times 2.650 \frac{\psi_o}{\Delta^{2/3}} = 3.533 \frac{\psi_o}{\Delta^{2/3}} \qquad (30)$$

To approximate the derivative $\psi_{\sim\eta}$ in equation (28), ψ is expanded at points i and ii by means of a Taylor's series about point 0. Terms involving $\psi_{\sim\sim\eta\eta}\big|_0$ may be omitted here, since the differential equation (10) shows this derivative to be identically zero at points on the sonic line. The values of ψ at i and ii can thus be written

$$\psi_i = \psi_0 - \Delta\, \psi_{\sim\eta}\big|_0 - \frac{\Delta^3}{3!}\, \psi_{\sim\sim\eta\eta\eta}\big|_0 + O(\Delta^4)$$

$$\psi_{ii} = \psi_0 - 2\Delta\, \psi_{\sim\eta}\big|_0 - \frac{(2\Delta)^3}{3!}\, \psi_{\sim\sim\eta\eta\eta}\big|_0 + O(\Delta^4)$$

Solution of these equations for $\psi_{\sim\eta}\big|_0$ gives, to the second order in Δ,

$$\psi_{\sim\eta}\big|_0 = \frac{1}{\Delta}\left(\frac{7}{6}\psi_0 - \frac{4}{3}\psi_i + \frac{1}{6}\psi_{ii}\right) \tag{31}$$

Substitution of expressions (30) and (31) into the boundary condition (28) gives the following finite-difference equation for the first point below the upper boundary:

$$\frac{4}{3}\psi_i - \frac{1}{6}\psi_{ii} - \left(\frac{7}{6} + 1.208\,\Delta^{1/3}\right)\psi_0 = 0 \tag{32}$$

Unlike the previous equations (20), (22), (23), and (27) this equation involves the value of Δ.

Lower points:

For a general point below the first lattice point, the situation is as represented in the sketch. The integral in the boundary condition (28) is here evaluated in three sections. The integral over the lattice interval from B to n-1 is evaluated on the basis of the asymptotic relation used before. The integral from n-1 to 1 is evaluated by assuming a linear variation in ψ over each of the included intervals and then integrating analytically. The linear assumption is sufficiently accurate here, since this entire middle section contributes only a relatively small portion of the complete integral. The integral from 1 to 0, which contains a singularity in the integrand at the point 0, is evaluated by expressing ψ as a cubic in terms of its value at the points 2, 1, 0, and -1 and then integrating analytically as before. The added accuracy of the cubic is required here, since this last section contributes by far the majority of the over-all value. The boundary condition (28) may thus be written

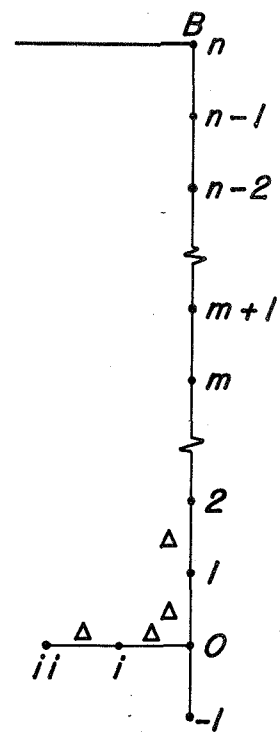

$$\underset{\eta}{\psi}(0,\tilde{\theta}) + 0.342\,(J_1+J_2+J_3) = 0 \qquad (33)$$

where the J's represent the three component integrals just described.

Proceeding to the details of the above procedure, the integral from B to n-1 is first written

$$J_1 \equiv \int_{\tilde{\theta}_w}^{\tilde{\theta}_w-\Delta} \frac{\psi_{\tilde{\theta}}(0,\tilde{\theta}')}{[n\Delta-(\tilde{\theta}_w-\tilde{\theta}')]^{2/3}}\, d\tilde{\theta}' = \frac{4\psi_{n-1}}{3\Delta^{2/3}} \int_0^1 \frac{\tau^{1/3}}{(n-\tau)^{2/3}}\, d\tau$$

where, as before, $\tau = (\tilde{\theta}_w-\tilde{\theta}')/\Delta$. This integral can be expressed, if desired, as the difference of two elliptic integrals of the first kind. For present purposes, however, it is more convenient (and sufficiently accurate) to expand $(n-\tau)^{-2/3}$ according to the binomial theorem and integrate termwise. This gives finally

$$J_1 = \frac{1}{(n\Delta)^{2/3}} \left(1 + \frac{8}{21n} + \frac{2}{9n^2} + \frac{160}{1053n^3} + \frac{55}{486n^4} + \cdots\right)\psi_{n-1} \qquad (34)$$

This expression is used, of course, only for $n \geq 2$.

On the basis of the assumption of a linear variation of ψ between adjacent lattice points, the integral from n-1 to 1 becomes

$$J_2 \equiv \int_{\tilde{\theta}_w-\Delta}^{\tilde{\theta}_w-(n-1)\Delta} \frac{\psi_{\tilde{\theta}}(0,\tilde{\theta}')}{[n\Delta-(\tilde{\theta}_w-\tilde{\theta}')]^{2/3}}\, d\tilde{\theta}' =$$

$$\sum_{m=1}^{n-2} \frac{\psi_{m+1}-\psi_m}{\Delta} \int_{\tilde{\theta}_w-(n-m-1)\Delta}^{\tilde{\theta}_w-(n-m)\Delta} \frac{1}{[n\Delta-(\tilde{\theta}_w-\tilde{\theta}')]^{2/3}}\, d\tilde{\theta}'$$

Carrying out the integration gives

$$J_2 = \frac{3}{\Delta^{2/3}} \sum_{m=1}^{n-2} \left[(m+1)^{1/3}-m^{1/3} \right] \left(\psi_m-\psi_{m+1} \right) \tag{35a}$$

This expression is valid for $n \geq 3$. (For $n = 2$, J_2 obviously does not exist.) For $n > 3$ it is convenient to rewrite the summation so that the value of ψ at a given point is not repeated in successive terms of the series. This is done by separating expression (35a) into two series (one with ψ_m and one with ψ_{m+1}), expanding these series, and then regrouping terms. The result is finally

$$J_2 = \frac{3}{\Delta^{2/3}} \left\{ \left[2^{1/3}-1 \right] \psi_1 + \sum_{m=2}^{n-2} \left[(m+1)^{1/3}-2m^{1/3} + (m-1)^{1/3} \right] \psi_m - \right.$$

$$\left. \left[(n-1)^{1/3}-(n-2)^{1/3} \right] \psi_{n-1} \right\} \tag{35b}$$

This expression is valid for $n \geq 4$.

To evaluate the integral from 1 to 0, ψ is represented within this interval by a cubic of the form

$$\psi = a + b \left(\frac{\tilde{\theta}_w-\tilde{\theta}}{\Delta} \right) + c \left(\frac{\tilde{\theta}_w-\tilde{\theta}}{\Delta} \right)^2 + d \left(\frac{\tilde{\theta}_w-\tilde{\theta}}{\Delta} \right)^3$$

where a, b, c, and d are determined such that ψ has the proper values at the points 2, 1, 0, and -1. This expression is to be substituted into the integral

$$J_3 \equiv \int_{\tilde{\theta}_w-(n-1)\Delta}^{\tilde{\theta}_w-n\Delta} \frac{\psi_{\tilde{\theta}}(0,\tilde{\theta}')}{[n\Delta-(\tilde{\theta}_w-\tilde{\theta}')]^{2/3}}\, d\tilde{\theta}'$$

The result is finally, after evaluation of the coefficients a, b, c, and d,

$$J_3 = \frac{-1}{\Delta^{2/3}}\left(\frac{2}{7}\psi_2 - \frac{87}{28}\psi_1 + \frac{33}{14}\psi_0 + \frac{13}{28}\psi_{-1}\right) \tag{36}$$

The finite-difference equation for a general point on the sonic line can now be obtained by replacing the J's in equation (33) by the expressions (34), (35), and (36) and using the previous expression (31) for the derivative $\psi_{\tilde{\eta}}\big|_0$. The result is a lengthy linear equation involving the value of ψ at the points i, ii, -1, 0, 1, 2, ..., n-1, n. Fortunately for the later relaxation work, the coefficients of the terms turn out to be relatively small for all points above the point 2.

Distribution of mesh points.- When an attempt is made to solve the present problem with a coarse mesh, it is soon found that most of the variation in ψ takes place in a relatively small region near the intersection of the shock polar and sonic line. To obtain a sufficiently accurate solution in a practicable length of time, it is therefore necessary to employ a graded lattice, that is, a lattice which has different spacing in different parts of the field. Figure 2 shows the distribution of lattice spacing found satisfactory in a typical case ($\tilde{\theta}_w = 1.6$). The particular arrangement shown here involves a total of 228 lattice points. For other values of $\tilde{\theta}_w$, the grading of the lattice follows the same general scheme. Obviously, however, the total number of lattice points must be increased as the upper boundary is moved farther from the shock polar.[7]

Formulas (34), (35), and (36), which are used to approximate the integral along the sonic line, presume the existence of lattice points at a uniform interval over the full distance from the upper boundary to the point in question. This condition is not fulfilled in a graded

[7]Occasionally, when two points on or adjacent to the shock polar fall very close together, one of the points is arbitrarily omitted. An expression for the omitted value of ψ, which is then necessary to complete the difference equation at neighboring points, is found by parabolic interpolation between the values at the available locations.

lattice such as that indicated in figure 2. Some modification of the method must therefore be made to obtain the finite-difference equation for a point on the sonic line in one of the regions of finer mesh. This requirement was satisfied by means of a simple averaging process in which the contribution of nonexistent fine-mesh points is replaced by an average contribution expressed in terms of ψ at bracketing points on the available coarser net. Since the contribution of individual points is small even for points only moderately removed from that at which the equation applies, a rather crude averaging process is sufficient in most cases. (The details need not be given here as they would soon become apparent to anyone working with the method.) When the averaging procedure would not be sufficiently accurate (as when the point at which the equation applies is near the line of demarcation between two different sized meshes), fictitious intermediate points are introduced into the coarser net and the value of ψ at these points is obtained from plots of the distribution of ψ along the sonic line.

Solution of Finite-Difference Equations

By the methods of the foregoing section, a finite-difference equation can be obtained for each lattice point in the hodograph plane. The result is a large number of simultaneous algebraic equations involving an equal number of unknown values of ψ. Since the number of unknowns in each equation is small, the equations lend themselves well to solution by relaxation techniques.[8]

The mechanics of the relaxation process have been well described by various authors (references 15, 16, 17, and 18) and need not be gone into here. For present purposes it was found satisfactory to take ψ_E in the boundary condition (16) equal to 10,000 and work with integer values of ψ throughout most of the field. The residuals in the relaxation process were eliminated to within limits of ± 2 (with due care, of course, that all residuals in any given area were not predominately of the same sign). To obtain satisfactory smoothness of the solution near the left-hand boundary in some examples, it was necessary in this region to work with values of ψ to 0.1 and eliminate residuals to within ± 0.5. Whenever the coefficients in the finite-difference

[8]It is interesting to note that, of the complete set of simultaneous equations, only two — those for the points on the shock polar and sonic line immediately adjacent to the point E — are not homogeneous. Only this fact prevents the solution of the complete set from being identically zero.

equations were relatively small, the corresponding terms were neglected in the point-by-point adjustment of ψ. The error so introduced was eliminated periodically by recomputing the residuals using all terms in the finite-difference equations. This procedure was particularly helpful in the case of the lengthy equations which apply at points on the sonic line. The transition between the various regions of the graded lattice, which is not often discussed in the literature, was accomplished by the use of overlapping fields in essentially the manner described in reference 28.

By means of the foregoing procedures, the boundary-value problem in the hodograph plane has been solved for values of $\tilde{\theta}_w$ of 1.3, 1.6, 2.4, and 4.2. These values correspond, respectively (see equation (18)), to values of the transonic similarity parameter ξ_0 of 1.058, 0.921, 0.703, and 0.484 as given previously in reference 1. As shown in the earlier paper, calculations for these values were sufficient to bridge the gap between the previous results of Guderley and Yoshihara at $\xi_0 = 0$ (reference 29) and the analytic results which can be obtained when the bow wave is attached and the flow is completely supersonic (reference 30). As an example of the solution in the hodograph plane, the variation of ψ for $\tilde{\theta}_w = 1.6$ is shown as a function of $\tilde{\eta}$ and $\tilde{\theta}$ in figure 3. (These results correspond to the results shown in the physical plane in fig. 2 of reference 1.) This figure shows clearly the rapid variation of ψ near the intersection of the shock polar and sonic line. The calculated values of ψ corresponding to figure 3 are listed in table I at the end of the report.

TRANSFORMATION TO PHYSICAL PLANE

Flow Field

The transformation from the hodograph plane to the physical plane is governed, in the small-disturbance theory, by the following equations (cf. reference 5):

$$dx = \frac{(\gamma+1)^{1/3}}{\rho_* a_*} (\eta \psi_\theta \, d\eta + \psi_\eta \, d\theta)$$

$$dy = \frac{1}{\rho_* a_*} (\psi_\eta \, d\eta + \psi_\theta \, d\theta) = \frac{1}{\rho_* a_*} d\psi$$

The second of these equations implies that, in a flow field determined according to the transonic small-disturbance theory, all streamlines appear as straight lines parallel to the horizontal axis. When expressed in terms of $\tilde{\eta}$ and $\tilde{\theta}$ the foregoing equations become

$$dx = \frac{(\gamma+1)^{1/3}}{\rho_* a_*} \sqrt{\frac{\eta_0}{2}} \left(2\tilde{\eta}\, \psi_{\tilde{\theta}}\, d\tilde{\eta} + \psi_{\tilde{\eta}}\, d\tilde{\theta}\right)$$

$$dy = \frac{1}{\rho_* a_*} \left(\psi_{\tilde{\eta}}\, d\tilde{\eta} + \psi_{\tilde{\theta}}\, d\tilde{\theta}\right) = \frac{1}{\rho_* a_*}\, d\psi$$

The length l of the wedge, which is equal to one-half the chord of the double-wedge profile, can be found by integrating the first of these equations over the upper boundary OB of the hodograph. (See sketch.) This gives

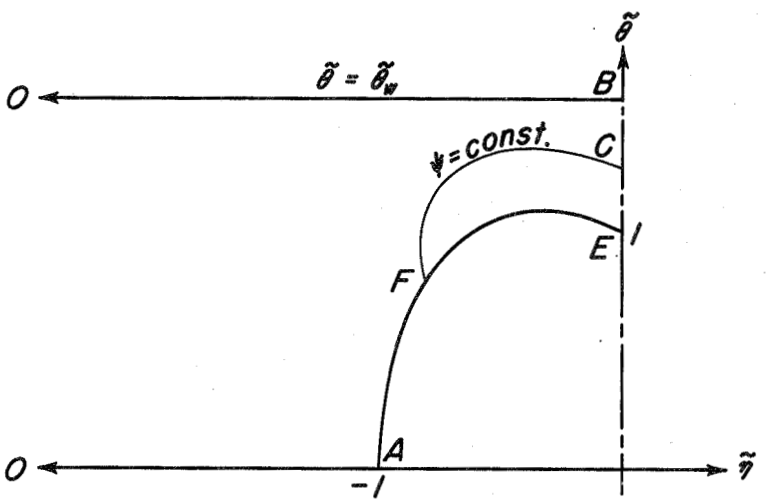

$$l = \frac{c}{2} = \frac{(\gamma+1)^{1/3}}{\rho_* a_*} \sqrt{\frac{\eta_0}{2}} \times 2 \int_{-\infty}^{0} \tilde{\eta}\, \psi_{\tilde{\theta}}(\tilde{\eta}, \tilde{\theta}_w)\, d\tilde{\eta}$$

With this relation the previous transformation equations can be put in the dimensionless form

$$d\left(\frac{x}{c}\right) = \frac{1}{4I_w} \left(2\tilde{\eta}\, \psi_{\tilde{\theta}}\, d\tilde{\eta} + \psi_{\tilde{\eta}}\, d\tilde{\theta}\right) \tag{37}$$

$$(\gamma+1)^{1/3} \sqrt{\frac{\eta_0}{2}}\, d\left(\frac{y}{c}\right) = \frac{1}{4I_w}\, d\psi \tag{38}$$

where I_w represents the integral

$$I_w = \int_{-\infty}^{0} \tilde{\eta}\, \psi_{\tilde{\theta}}(\tilde{\eta}, \tilde{\theta}_w)\, d\tilde{\eta} \tag{39}$$

To obtain the flow field in the form given in reference 1, equation (38) must be rewritten in terms of the ordinate function

$$\tilde{Y} \cong [(\gamma+1)(t/c)]^{1/3} \left(\frac{y}{c}\right)$$

The result, derived with the aid of the relation

$$\tilde{\theta}_w = \sqrt{2}\,\frac{t/c}{\eta_o^{2/3}}$$

is

$$d\tilde{Y} \cong [(\gamma+1)(t/c)]^{1/3}\, d\left(\frac{y}{c}\right) = \frac{(2\tilde{\theta}_w)^{1/3}}{4I_w}\, d\psi \tag{40a}$$

Integrating this relation, subject to the condition that $\tilde{Y} = 0$ when $\psi = 0$, gives

$$\tilde{Y} \cong [(\gamma+1)(t/c)]^{1/3} \left(\frac{y}{c}\right) = \frac{(2\tilde{\theta}_w)^{1/3}}{4I_w}\, \psi \tag{40b}$$

To utilize the foregoing equations for actual computations, it is first necessary to evaluate I_w. Since numerical values of ψ are available in the hodograph only for $-\beta \leq \tilde{\eta} \leq 0$, the evaluation must be carried out in two parts as follows:

$$I_w = \int_{-\beta}^{0} \tilde{\eta}\, \underset{\sim}{\psi}_{\theta}(\tilde{\eta},\tilde{\theta}_w)\, d\tilde{\eta} + \int_{-\infty}^{-\beta} \tilde{\eta}\, \underset{\sim}{\psi}_{\theta}(\tilde{\eta},\tilde{\theta}_w)\, d\tilde{\eta} \tag{41}$$

The first integral is evaluated from the results of the numerical solution by mechanical integration of a curve of $\tilde{\eta}\, \underset{\sim}{\psi}_{\theta}(\tilde{\eta},\tilde{\theta}_w)$ versus $\tilde{\eta}$. The values of the derivative used for this purpose are obtained from the equation

$$\underset{\sim}{\psi}_{\theta}\Big|_0 = \frac{1}{\Delta}\left(-\frac{4}{3}\psi_1 + \frac{1}{6}\psi_2\right) \tag{42}$$

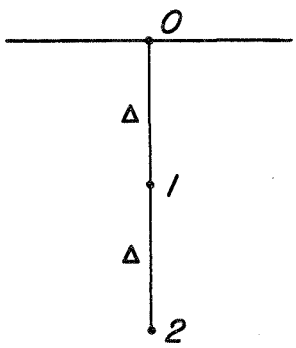

where the notation is as shown in the sketch. This equation is derived in the same way as equation (31), except that ψ_0 is here taken equal to zero in accord with the boundary condition.[9] It can be shown from Guderley's singular solution for corner flow that for small negative values of $\tilde{\eta}$ the curve of $\tilde{\eta}\,\psi_{\tilde{\theta}}(\tilde{\eta},\tilde{\theta}_w)$ must behave essentially as $|\tilde{\eta}|^{3/2}$. This result is useful in fairing the numerical results near $\tilde{\eta} = 0$. The first integral in equation (41) contributes by far the majority (about 99 percent) of the total value of I_w.

To evaluate the second integral in equation (41) use in again made of the asymptotic solution (21). For this purpose, the constant B is determined such that the value of $\psi_{\tilde{\theta}}$ given by the asymptotic solution matches the numerically determined value at the point $(-\beta,\tilde{\theta}_w)$. Substitution of equation (21) into the second integral of equation (41) then gives

$$\int_{-\infty}^{-\beta} \tilde{\eta}\,\psi_{\tilde{\theta}}(\tilde{\eta},\tilde{\theta}_w)\,d\tilde{\eta} = -\frac{\beta^{1/4}\,\psi_{\tilde{\theta}}(-\beta,\tilde{\theta}_w)}{\exp\left[-\frac{\pi}{3\tilde{\theta}_w}(2\beta)^{3/2}\right]} \times \int_{-\infty}^{-\beta}(-\tilde{\eta})^{3/4}\exp\left[-\frac{\pi}{3\tilde{\theta}_w}(-2\tilde{\eta})^{3/2}\right]d\tilde{\eta} \qquad (43)$$

where $\psi_{\tilde{\theta}}(-\beta,\tilde{\theta}_w)$ is determined from equation (42) applied at $\tilde{\eta} = -\beta$. The integral on the right is transformed through the substitution

$$\frac{\pi}{3\tilde{\theta}_w}(-2\tilde{\eta})^{3/2} = \omega$$

[9]The fact that the second derivative $\psi_{\tilde{\theta}\tilde{\theta}}|_0$ may be taken as zero in the present derivation follows from the boundary condition and the differential equation (10).

which gives

$$\int_{-\infty}^{-\beta} (-\tilde{\eta})^{3/4} \exp\left[-\frac{\pi}{3\theta_w}(-2\eta)^{3/2}\right] d\tilde{\eta} =$$

$$\frac{1}{3\times 2^{3/4}} \left(\frac{3\tilde{\theta}_w}{\pi}\right)^{7/6} \int_{\frac{\pi}{3\tilde{\theta}_w}(2\beta)^{3/2}}^{\infty} \omega^{1/6} e^{-\omega} d\omega$$

The integral here is then found with sufficient accuracy by means of the following asymptotic formula, valid for large values of the lower limit (see pp. 95-96 of reference 31):

$$\int_z^{\infty} \omega^{\nu-1} e^{-\omega} d\omega \cong z^{\nu-1} e^{-z}$$

Equation (43) thus reduces finally to

$$\int_{-\infty}^{-\beta} \tilde{\eta}\, \psi_{\tilde{\theta}}\left(\tilde{\eta},\tilde{\theta}_w\right) d\tilde{\eta} = -\left(\frac{\beta}{2}\right)^{1/2} \frac{\tilde{\theta}_w}{\pi} \psi_{\tilde{\theta}}(-\beta,\tilde{\theta}_w) \tag{44}$$

With the value of I_w known, equations (37) and (40) can be used to obtain the coordinates x/c and $\tilde{Y}$ corresponding to any point in the $\tilde{\eta},\tilde{\theta}$ plane. The value of $\tilde{Y}$ is obtained by direct substitution of the appropriate value of ψ into equation (40b). The value of x/c must be found by suitable integration of equation (37). The location of the vertex A of the shock wave is found, for example, by integrating equation (37) along the line OA in the hodograph. (See sketch on p. 30.) If the leading edge O is taken as the origin in the physical plane, this gives

$$\left(\frac{x}{c}\right)_A = \frac{1}{2I_w} \int_{-\infty}^{-1} \tilde{\eta}\, \psi_{\tilde{\theta}}(\tilde{\eta},0)\, d\tilde{\eta} \tag{45}$$

The integral here is evaluated in two parts following the procedure previously used in determining I_w.

For the abscissa of a point F on the shock wave, equation (37) gives

$$\left(\frac{x}{c}\right)_F = \left(\frac{x}{c}\right)_A + \frac{1}{4I_w} \int_A^F \left(2\tilde{\eta}\, \psi_{\tilde{\theta}}\, d\tilde{\eta} + \psi_{\tilde{\eta}}\, d\tilde{\theta}\right)$$

where the integration is now taken from A to F along the shock polar. For purposes of numerical evaluation, the integrand here can be simplified by writing

$$2\tilde{\eta}\,\psi_{\tilde{\theta}}\,d\tilde{\eta} + \psi_{\tilde{\eta}}\,d\tilde{\theta} = \frac{2\tilde{\eta}\,\psi_{\tilde{\theta}}\,d\tilde{\eta} + \psi_{\tilde{\eta}}\,d\tilde{\theta}}{\psi_{\tilde{\eta}}\,d\tilde{\eta} + \psi_{\tilde{\theta}}\,d\tilde{\theta}}\,d\psi$$

$$= \frac{2\tilde{\eta} + (\psi_{\tilde{\eta}}/\psi_{\tilde{\theta}})(d\tilde{\theta}/d\tilde{\eta})}{(\psi_{\tilde{\eta}}/\psi_{\tilde{\theta}}) + (d\tilde{\theta}/d\tilde{\eta})}\,d\psi$$

If $(\psi_{\tilde{\eta}}/\psi_{\tilde{\theta}})$ and $(d\tilde{\theta}/d\tilde{\eta})$ are replaced by the appropriate functions of $\tilde{\eta}$ from equations (14), there results finally

$$\left(\frac{x}{c}\right)_F = \left(\frac{x}{c}\right)_A + \frac{1}{4I_w}\int_0^{\psi_F} \sqrt{1+\tilde{\eta}}\,d\psi \tag{46}$$

The integral in this equation is evaluated by plotting a curve of ψ versus $\sqrt{1+\tilde{\eta}}$ from the numerical results along the shock polar and carrying out the necessary integration by mechanical means.

The abscissa of a point on the sonic line is found by integrating equation (37) along the $\tilde{\theta}$ axis from B to C. Since point B is situated in the physical plane at $x/c = 1/2$, this gives

$$\left(\frac{x}{c}\right)_C = \frac{1}{2} + \frac{1}{4I_w}\int_{\tilde{\theta}_w}^{\tilde{\theta}_C} \psi_{\tilde{\eta}}(0,\tilde{\theta})\,d\tilde{\theta} \tag{47}$$

The integral here is evaluated by mechanical integration of a curve of $\psi_{\tilde{\eta}}(0,\tilde{\theta})$ versus $\tilde{\theta}$, where $\psi_{\tilde{\eta}}(0,\tilde{\theta})$ is found from equation (31). As can be seen from equation (28) and relation (29), $\psi_{\tilde{\eta}}(0,\tilde{\theta})$ in the vicinity of point B varies essentially as $(\tilde{\theta}_w-\tilde{\theta})^{2/3}$. This fact is of use in drawing the curve of $\psi_{\tilde{\eta}}(0,\tilde{\theta})$ near $\tilde{\theta}=\tilde{\theta}_w$. It can further be seen with the aid of equation (40b) that near the shoulder of the wedge the transformed sonic line has the form

$$\left(\frac{x}{c}\right)_C - \frac{1}{2} \sim \tilde{Y}^{5/4}$$

This relation is useful in establishing the detailed shape of the sonic line in the physical plane. It shows, in particular, that the sonic line will have a vertical tangent and an infinite curvature at the shoulder of the wedge.

Pressure Distribution and Drag

To complete the analysis of the front wedge, it is left to determine the pressure distribution and drag. Integration of equation (37) gives for the chordwise location on the wedge of a given value of $\tilde{\eta}$

$$\frac{x}{c} = \frac{1}{2I_w} \int_{-\infty}^{\tilde{\eta}} \tilde{\eta}\, \underset{\sim}{\psi}_{\theta}(\tilde{\eta},\tilde{\theta}_w)\, d\tilde{\eta}$$

or

$$\frac{x}{c} = \frac{1}{2} + \frac{1}{2I_w} \int_{0}^{\tilde{\eta}} \tilde{\eta}\, \underset{\sim}{\psi}_{\theta}(\tilde{\eta},\tilde{\theta}_w)\, d\tilde{\eta} \tag{48}$$

The speed parameter $\xi \cong (M^2-1)/[(\gamma+1)(t/c)]^{2/3}$ which was used to present the results in reference 1, is related to $\tilde{\eta}$ by the following equation, derived from equations (20) and (21) of reference 1 and equations (1), (9), and (18) of the present paper:

$$\xi = \xi_o \tilde{\eta} = \frac{2^{1/3}}{\tilde{\theta}_w^{2/3}} \tilde{\eta} \tag{49}$$

With these equations, the distribution of ξ as a function of x/c is readily determined. The integration of equation (48) is carried out by mechanical means using the same curve previously employed to determine I_w. To fair the resulting ξ curve in the vicinity of the shoulder, use is again made of Guderley's analytical findings, which show that in this vicinity

$$\xi \sim \left(\frac{1}{2} - \frac{x}{c}\right)^{2/5}$$

The chordwise distribution of the generalized pressure coefficient

$$\tilde{C}_p \cong \left[(\gamma+1)^{1/3}/(t/c)^{2/3}\right] C_p$$

is related to the distribution of ξ by the following equation taken from pages 16 and 23 of reference 1:

$$\tilde{C}_p = -2(\xi - \xi_o) \tag{50}$$

To find the portion of the generalized drag coefficient

$$\tilde{c}_d \cong [(\gamma+1)/(t/c)^{5/3}]\, c_d$$

contributed by the front half of the double-wedge profile, equation (13a) of reference 1 gives

$$\tilde{c}_{d_f} = 2 \int_0^{1/2} \tilde{C}_p \, d\left(\frac{x}{c}\right) \tag{51}$$

To allow for the singularity in $\tilde{C}_p$ at the leading edge, the integration is best carried out directly in terms of the hodograph variables. To this end, substitution from equations (37), (49), and (50) gives

$$\tilde{c}_{d_f} = 2\,\xi_0 \left[1 - \frac{1}{I_w} \int_{-\infty}^{0} \tilde{\eta}^2 \, \psi_{\tilde{\theta}}(\tilde{\eta},\tilde{\theta}_w)\, d\tilde{\eta} \right] \tag{52}$$

The integration here is performed in two parts following procedures parallel to those used in evaluating I_w.

CHARACTERISTICS CONSTRUCTION OVER REAR OF AIRFOIL

The characteristics in the $\tilde{\eta},\tilde{\theta}$ plane ($\tilde{\eta}>0$) are given by the following relation obtained from equations (3) and (9):

$$\tilde{\theta} = \text{const.} \pm \frac{2^{3/2}}{3} \tilde{\eta}^{3/2} \tag{53}$$

The corresponding directions of the Mach lines in the generalized physical plane, as determined from this relation and the transformation equations (37) and (40a), are

$$\frac{d\tilde{Y}}{d(x/c)} = \pm \frac{(2\tilde{\theta}_w)^{1/3}}{(2\tilde{\eta})^{1/2}} \tag{54}$$

To the present order of approximation, therefore, the slope of the Mach lines is independent of the local inclination $\tilde{\theta}$. This is consistent with the previous result that the streamlines must appear in the physical plane as horizontal straight lines. As a consequence, the construction of the Mach net over the rear of the airfoil is particularly simple in the small-disturbance theory.

To aid in the construction, the equations for the characteristics in the $\tilde{\eta},\tilde{\theta}$ plane can be conveniently written in the form

$$\tilde{\theta} = \tilde{\Theta}_u + \frac{2^{3/2}}{3}\tilde{\eta}^{3/2}$$

$$\tilde{\theta} = \tilde{\Theta}_d - \frac{2^{3/2}}{3}\tilde{\eta}^{3/2}$$

The symbols $\tilde{\Theta}_u$ and $\tilde{\Theta}_d$ denote, respectively, the ordinates at which the upgoing and downgoing characteristics through a given point $(\tilde{\eta},\tilde{\theta})$ intersect the vertical axis. Elimination of $\tilde{\theta}$ between these equations gives

$$\tilde{\eta} = \frac{3^{2/3}}{2^{5/3}}(\tilde{\Theta}_d - \tilde{\Theta}_u)^{2/3} \tag{55}$$

which can be substituted into equation (54) to obtain

$$\frac{d\tilde{Y}}{d(x/c)} = \pm\left(\frac{4\tilde{\theta}_w/3}{\tilde{\Theta}_d - \tilde{\Theta}_u}\right)^{1/3} \tag{56}$$

This is the basic relation for the characteristics construction in the physical plane.

The construction of the Mach net itself follows a simple lattice-point procedure (cf. reference 32). By identifying each Mach line with its appropriate value of $\tilde{\Theta}_u$ or $\tilde{\Theta}_d$, the value of $d\tilde{Y}/d(x/c)$ at the intersection of any two Mach lines can easily be determined from equation (56) (or its graphical equivalent). The basic construction necessary to locate an unknown point c from the location of two known

points a and b is then as indicated in the sketch. The construction proceeds rapidly since, as pointed out, variations in the inclination of

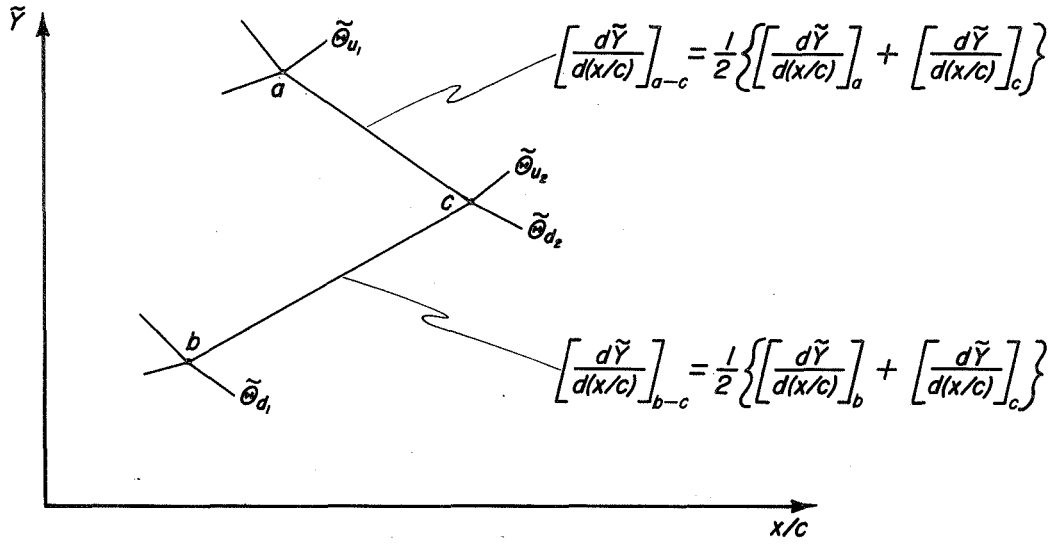

flow need not be considered in establishing the direction of the Mach lines. Where desired, the value of $\tilde{\theta}$ can be found from the relation

$$\tilde{\theta} = \frac{\tilde{\Theta}_d + \tilde{\Theta}_u}{2} \tag{57}$$

The corresponding value of $\tilde{\eta}$ is given by equation (55).[10]

Figure 4 shows a typical Mach net constructed by stepwise application of the foregoing procedure. This net is for the case of $\tilde{\theta}_w = 1.6$ ($\xi_o = 0.921$) and corresponds to the flow field shown for the front of the airfoil in figure 2 of reference 1. The construction is

---

[10] In practice, the construction is actually carried out most easily in a plane of $\tilde{Y}/(2\tilde{\theta}_w)^{1/3}$ versus x/c with the slope of the Mach lines given by

$$\frac{d[\tilde{Y}/(2\tilde{\theta}_w)^{1/3}]}{d(x/c)} = \pm \left(\frac{2/3}{\tilde{\Theta}_d - \tilde{\Theta}_u}\right)^{1/3}$$

This allows a single graph of slope versus $(\tilde{\Theta}_d - \tilde{\Theta}_u)$ to suffice for all values of $\tilde{\theta}_w$. It also provides somewhat more convenient proportions for the construction of the Mach net.

begun at the shoulder of the airfoil ($x/c = 1/2$, $\tilde{Y} = 0$) with the values of $\tilde{\Theta}_u$ selected to provide approximately equal spacing between the Mach lines of the expansion fan. From the shoulder, the construction is carried outward to the sonic line and then inward to the rear surface of the airfoil. The drawing of the Mach line segments adjoining the sonic line might appear at first to offer some difficulty, since a linear average is obviously unreliable to determine a mean inclination in this vicinity. Actually, no trouble is encountered from this source, since the point at which each Mach line meets the sonic line is already known from the hodograph solution for the subsonic field. The construction of the last segment approaching the sonic line thus reduces to a matter of simply connecting two known points. The slope of the first segment leaving the sonic line is found by either (a) multiplying the slope of the approaching segment by -1, or (b) determining a mean inclination based on the easily demonstrated fact that a Mach line in the vicinity of the sonic line behaves essentially as a semicubical parabola.[11] It is immaterial to the final result which procedure is used. The identity of the Mach lines reflected from the rear surface of the airfoil is determined from equation (57) plus the boundary condition that at this surface $\tilde{\theta} = -\tilde{\theta}_w$. As can be seen by comparing figure 4 of the present report with figure 2 of reference 1, only a relatively small portion of the sonic line need be known to determine conditions on the rear of the airfoil.

REMARKS ON ACCURACY OF SOLUTION

Quantitative statements with regard to the accuracy of the present results are difficult to make. Fortunately, however, a check on the accuracy of the solution is available in the work itself. This check derives from the fact that, in the subsonic portion of the field, the calculated location of a given velocity in the physical plane should, theoretically, be independent of the path of integration which is followed in the hodograph. Thus, for example, the position of the velocity $\tilde{\eta} = 0$, $\tilde{\theta} = 1$, which defines the point of intersection E of the shock wave and sonic line, should be the same irrespective of whether it is found from equations (45) and (46)

$$\left(\frac{x}{c}\right)_E = \frac{1}{2I_w} \int_{-\infty}^{-1} \tilde{\eta}\, \psi_{\tilde{\theta}}(\tilde{\eta},0)\, d\tilde{\eta} + \frac{1}{4I_w} \int_0^{\psi_E} \sqrt{1+\tilde{\eta}}\, d\psi \qquad (58)$$

or from equation (47)

[11] The latter possibility was pointed out to the authors by Gottfried Guderley.

$$\left(\frac{x}{c}\right)_E = \frac{1}{2} + \frac{1}{4I_w} \int_{\tilde{\theta}_w}^{1} \psi_{\tilde{\eta}}(0,\tilde{\theta})\, d\tilde{\theta} \qquad (59)$$

Actually, as was observed in connection with figure 1 of reference 1, the results of the two determinations show a small discrepancy. Such a result would be expected in any finite-difference solution.

Discrepancies of the type noted can arise from two sources: (1) numerical inaccuracies in the relaxation solution of the finite-difference equations or in the transformation to the physical plane; (2) inaccuracies caused by the fact that the finite-difference equations themselves are not an exact representation of the boundary-value problem for the original partial differential equation. Experience with various refinements in the calculations indicates that the discrepancies here are primarily of the latter origin. Early computations with a coarse lattice and relatively crude finite-difference equations showed a considerable gap between the shock wave and the end of the sonic line. Increasing refinements in the grading of the lattice and in the derivation of certain of the finite-difference equations gave progressive improvement in reducing this gap. This improvement came about primarily as a result of progressive reduction in the value of the integral I_w, the other integrals in equations (58) and (59) being relatively unaffected by the refinements in the calculations. Indications are that, in the results which were taken as final, the values of $|\psi_{\tilde{\theta}}(\tilde{\eta},\tilde{\theta}_w)|$ and hence of I_w are still somewhat too large. This means (see equation (40b)) that the ordinates of the shock wave and sonic line are probably somewhat smaller than they should be. The same is probably true, in general, of the corresponding values of $|x/c|$. Calculations of the chordwise distribution of $\tilde{\eta}$ on the surface of the airfoil are, however, considerably more precise, since the errors in the two integrals in equation (48) tend to compensate. The refinements in the computations were, in fact, carried to the point where further betterment caused only negligible change in the pressure distribution and over-all drag. Further evidence of the accuracy of the results in this regard is provided by the ease with which the computed values fair into the results of Guderley and Yoshihara at $\xi_o = 0$ and into the analytical curves which are available when the bow wave is attached and the flow is completely supersonic. (See figs. 4 and 6 of reference 1.)

Ames Aeronautical Laboratory
National Advisory Committee for Aeronautics
Moffett Field, Calif., Oct. 8, 1951

REFERENCES

1. Vincenti, Walter G., and Wagoner, Cleo B.: Transonic Flow Past a Wedge Profile With Detached Bow Wave - General Analytical Method and Final Calculated Results. NACA TN 2339, 1951.

2. Bryson, Arthur Earl, Jr.: An Experimental Investigation of Transonic Flow Past Two-Dimensional Wedge and Circular-Arc Sections Using a Mach-Zehnder Interferometer. NACA TN 2560, 1951.

3. Liepmann, H. W., and Bryson, A. E., Jr.: Transonic Flow Past Wedge Sections. Jour. Aero. Sci., vol. 17, no. 12, Dec. 1950, pp. 745-755.

4. Frankl, F.: On the Problems of Chaplygin for Mixed Sub- and Supersonic Flows. NACA TM 1155, 1947.

5. Guderley, K. Gottfried: Considerations of the Structure of Mixed Subsonic-Supersonic Flow Patterns. Tech. Rept. F-TR-2168-ND, AAF, Air Materiel Command (Wright Field), Oct. 1947.

6. Guderley, K. Gottfried: New Aspects of Transonic Flow Theory. ATI Tech. Data Digest, vol. 12, no. 9, 1 Nov. 1947.

7. Busemann, Adolf: A Review of Analytical Methods for the Treatment of Flows with Detached Shocks. NACA TN 1858, 1949.

8. Tricomi, F.: On Linear Partial Differential Equations of the Second Order of Mixed Type. Trans. A9-T-26, Grad. Div. of Appl. Math., Brown University, 1948.

9. Green, J. R., and Southwell, R. V.: Relaxation Methods Applied to Engineering Problems. IX - High-Speed Flow of Compressible Fluid Through a Two-Dimensional Nozzle. Phil. Trans. Roy. Soc. London, ser. A, no. 808, vol. 239, April 1944, pp. 367-386.

10. Emmons, Howard W.: The Theoretical Flow of a Frictionless, Adiabatic, Perfect Gas Inside of a Two-Dimensional Hyperbolic Nozzle. NACA TN 1003, 1946.

11. O'Brien, George G., Hyman, Morton A., and Kaplan, Sidney: A Study of the Numerical Solution of Partial Differential Equations. Jour. Math. and Phys., vol. XXIX, no. 4, Jan. 1951, pp. 223-251.

12. Whittaker, E. T., and Watson, G. N.: A Course of Modern Analysis. Cambridge, Eng., The University Press, 1945.

13. Guderley, K. Gottfried: On the Transition from a Transonic Potential Flow to a Flow with Shocks. Tech. Rept. F-TR-2160-ND, AAF, Air Materiel Command (Wright Field), Aug. 1947.

14. von Kármán, Theodore: The Similarity Law of Transonic Flow. Jour. Math. and Phys., vol. 26, no. 3, Oct. 1947, pp. 182-190.

15. Emmons, Howard W.: The Numerical Solution of Partial Differential Equations. Quart. Appl. Math., vol. II, no. 3, Oct. 1944, pp. 173-195.

16. Fox, L.: A Short Account of Relaxation Methods. Quart. Jour. Mech. and Appl. Math., vol I, pt. 3, Sept. 1948, pp. 253-280.

17. Shaw, F. S.: Numerical Solutions of Boundary Value Problems by Relaxation Methods. Numerical Methods of Analysis in Engineering, L. E. Grinter, ed., Macmillan Co., N. Y., 1949, pp. 49-65.

18. Southwell, R. V.: Relaxation Methods in Theoretical Physics. Oxford, The Clarendon Press, 1946.

19. Bickley, W. G.: Finite Difference Formulae for the Square Lattice Quart. Jour. Mech. and Appl. Math., vol. I, pt. 1, Mar. 1948. pp. 35-42.

20. Fox, L.: Some Improvements in the Use of Relaxation Methods for the Solution of Ordinary and Partial Differential Equations. Proc., Royal Soc. London, ser. A, vol. 190, no. A 1020, June 17, 1947, pp. 31-59.

21. Woods, L. C.: Improvements to the Accuracy of Arithmetical Solutions to Certain Two-Dimensional Field Problems. Quart. Jour. Mech. and Appl. Math., vol. III, pt. 3, Sept. 1950, pp. 349-363.

22. Watson, G. N.: A Treatise on the Theory of Bessel Functions. 2nd ed., Cambridge, The University Press, 1948.

23. Wu, Chung-Hua: Formulas and Tables of Coefficients for Numerical Differentiation with Function Values Given at Unequally Spaced Points and Application to Solution of Partial Differential Equations. NACA TN 2214, 1950.

24. Fox, L.: Solution by Relaxation Methods of Plane Potential Problems with Mixed Boundary Conditions. Quart. Appl. Math., vol. II, no. 3, Oct. 1944, pp. 251-257.

25. Fox, L.: The Numerical Solution of Elliptic Differential Equations When the Boundary Conditions Involve a Derivative. Phil. Trans. Roy. Soc. London, ser. A, no. 849, vol. 242, 3 May 1950, pp. 345-378.

26. Guderley, K. Gottfried: Singularities at the Sonic Velocity. Tech. Rept. F-TR-1171-ND, Air Materiel Command, U. S. Air Force, June 1948.

27. Jahnke, Eugene, and Emde, Fritz: Tables of Functions With Formulae and Curves. Dover Publications, N. Y., 4th ed., 1945.

28. Tasny-Tschiassny, L.: The Triangulation of a Two Dimensional Continuum for the Purpose of the Approximate Solution of Second-Order Partial Differential Equations. Jour. App. Phys., vol. 20, no. 5, May 1949, pp. 419-424.

29. Guderley, K. Gottfried, and Yoshihara, H.: The Flow Over a Wedge Profile at Mach Number 1. Jour. Aero. Sci., vol. 17, no. 11, Nov. 1950, pp. 723-735.

30. Tsien, Hsue-Shen, and Baron, Judson R.: Airfoils in Slightly Supersonic Flow. Jour. Aero. Sci., vol. 16, no. 1, Jan. 1949, pp. 55-61.

31. Magnus, Wilhelm, and Oberhettinger, Fritz: Formulas and Theorems for the Special Functions of Mathematical Physics. Chelsea Publishing Co., N. Y., 1949.

32. Isenberg, J. S.: The Method of Characteristics in Compressible Flow. Part I (Steady Supersonic Flow). Tech. Rept. F-TR-1173-A-ND, Air Materiel Command (Wright Field), Dec. 1947.

TABLE I.- CALCULATED VALUES OF ψ FOR $\tilde{\theta}_w = 1.6$ ($\xi_o = 0.921$)

$-\tilde{\eta}$	$\tilde{\theta}$	ψ	$-\tilde{\eta}$	$\tilde{\theta}$	ψ	$-\tilde{\eta}$	$\tilde{\theta}$	ψ	$-\tilde{\eta}$	$\tilde{\theta}$	ψ
0	1.5	198	0.1	1.1	4591	0.45	1.25	1691	1.1	0.3	128
	1.4	527		1.075	5642		1.2	2004		.2	85
	1.3	1013		1.05	7132		1.15	2324		.1	43
	1.25	1359		1.0436	7621		1.1	2621			
	1.2	1822					1.0754	2748	1.2	1.4	98
	1.15	2480	.125	1.125	3971					1.2	176
	1.125	2927		1.1	4763	.5	1.5	394		1.0	219
	1.1	3502		1.075	5822		1.4	811		.8	220
	1.075	4272		1.0523	7130		1.3	1268		.7	207
	1.0625	4773					1.2	1755		.6	187
	1.05	5375	.15	1.25	1928		1.1	2196		.5	161
	1.375	6109		1.2	2559		1.0607	2313		.4	132
	1.025	7040		1.15	3467					.3	101
	1.0125	8267		1.125	4082	.6	1.5	329		.2	68
				1.1	4869		1.4	662		.1	34
.0125	1.0625	5003		1.075	5899		1.3	997			
	1.05	5644		1.0603	6664		1.2	1312	1.3	.6	137
	1.0375	6433					1.1	1552		.5	119
	1.025	7441	.175	1.125	4141		1.0119	1633		.4	99
	1.0125	8782		1.1	4902					.3	76
	1.0062	9656		1.075	5870	.7	1.5	258		.2	52
				1.0673	6223		1.4	511		.1	26
.025	1.125	3168					1.3	750			
	1.1	3805	.2	1.5	389		1.2	957	1.4	1.4	48
	1.075	4666		1.4	875		1.1	1101		1.2	87
	1.0625	5228		1.3	1565		1.0	1149		1.0	110
	1.05	5909		1.25	2042		.9311	1120		.8	114
	1.0375	6751		1.2	2679					.6	101
	1.025	7833		1.15	3567	.8	1.4	377		.4	74
	1.0121	9339		1.125	4148		1.2	689		.2	39
				1.1	4862		1.1	785			
.0375	1.0625	5447		1.0733	5810		1.0	822	1.6	1.4	23
	1.05	6165					.9	798		1.2	42
	1.0375	7057	.225	1.125	4100					1.0	54
	1.025	8205		1.1	4753	.8032	.8	720		.8	57
	1.0179	9025		1.0784	5420					.6	51
						.8581	.7	534		.4	38
.05	1.25	1568	.25	1.25	2092					.2	20
	1.2	2100		1.2	2699	.9	1.0	593			
	1.15	2872		1.15	3504		.9	585	1.8	1.4	10
	1.125	3403		1.125	4005		.8	545		1.2	19
	1.1	4097		1.1	4588		.7	481		1.0	25
	1.075	5041		1.0825	5046					.8	27
	1.0625	5657				.9003	.6	406		.6	24
	1.05	6407	.275	1.125	3868					.4	18
	1.0375	7343		1.1	4379	.9331	.5	307		.2	10
	1.0234	8729		1.0856	4704						
						.9583	.4	228	2.0	1.4	5
.0625	1.0625	5854	.3	1.5	435					1.2	9
	1.05	6630		1.4	948	.9770	.3	162		1.0	11
	1.0375	7601		1.3	1630					.8	12
	1.0288	8440		1.25	2072	.9899	.2	104		.6	12
				1.2	2620					.4	9
.075	1.125	3622		1.15	3301	.9975	.1	52		.2	5
	1.1	4365		1.1	4134						
	1.075	5374		1.0877	4357	1.0	1.4	197			
	1.0625	6034					1.2	352			
	1.05	6830	.35	1.25	1990		1.0	427			
	1.0375	7824		1.2	2460		.9	428			
	1.0339	8158		1.15	3007		.8	407			
				1.1	3618		.7	369			
.0875	1.0625	6194		1.0884	3763		.6	321			
	1.05	6999					.5	267			
	1.0388	7889	.4	1.5	435		.4	211			
				1.4	921						
.1	1.5	305		1.3	1509	1.1	.8	302			
	1.4	720		1.25	1857		.7	279			
	1.3	1330		1.2	2246		.6	247			
	1.25	1764		1.15	2669		.5	210			
	1.2	2356		1.1	3099		.4	170			
	1.15	3220		1.0844	3225						
	1.125	3815									

NACA

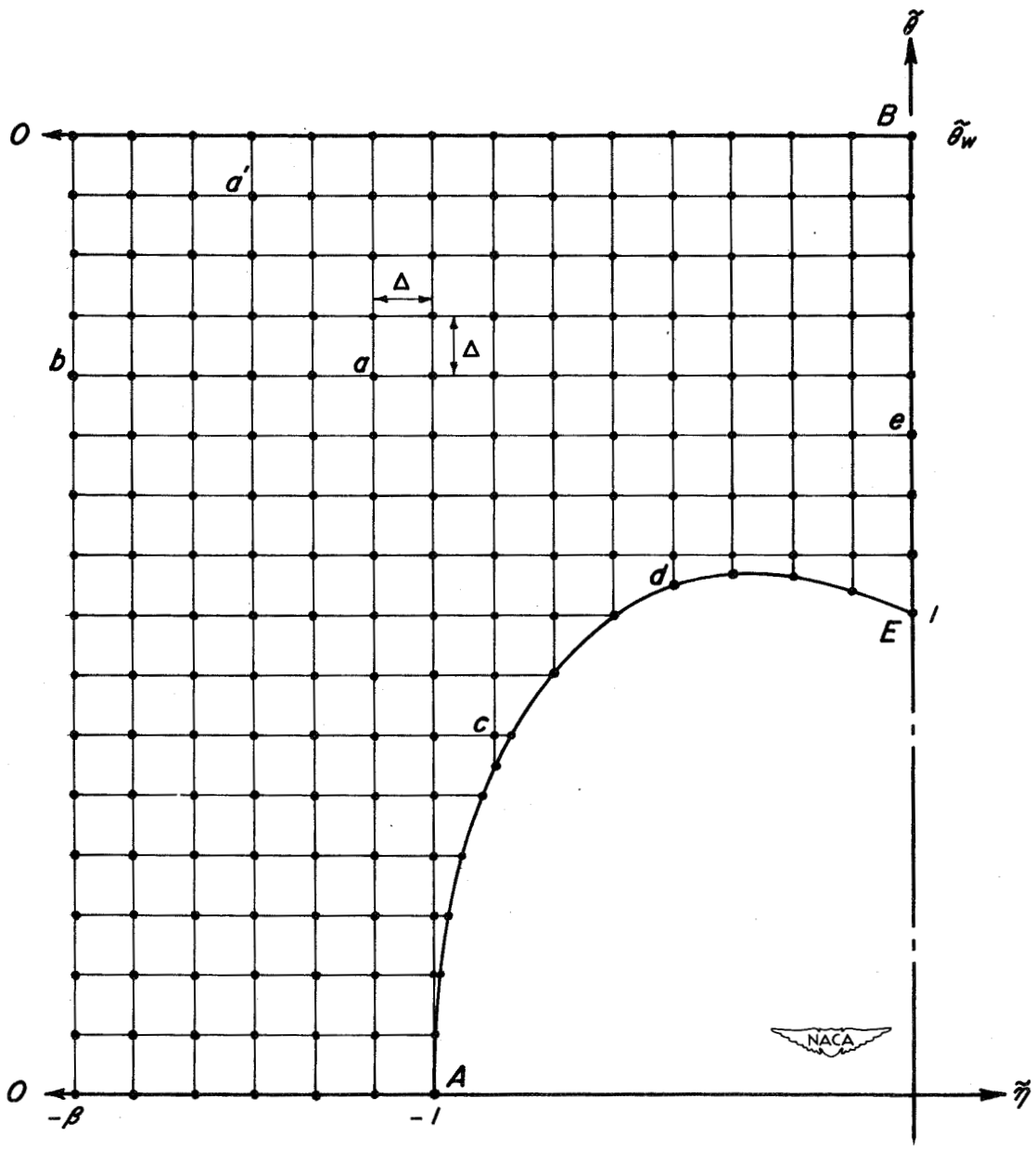

Figure 1.– Illustrative finite-difference lattice in the $\tilde{\eta}\tilde{\theta}$ plane.

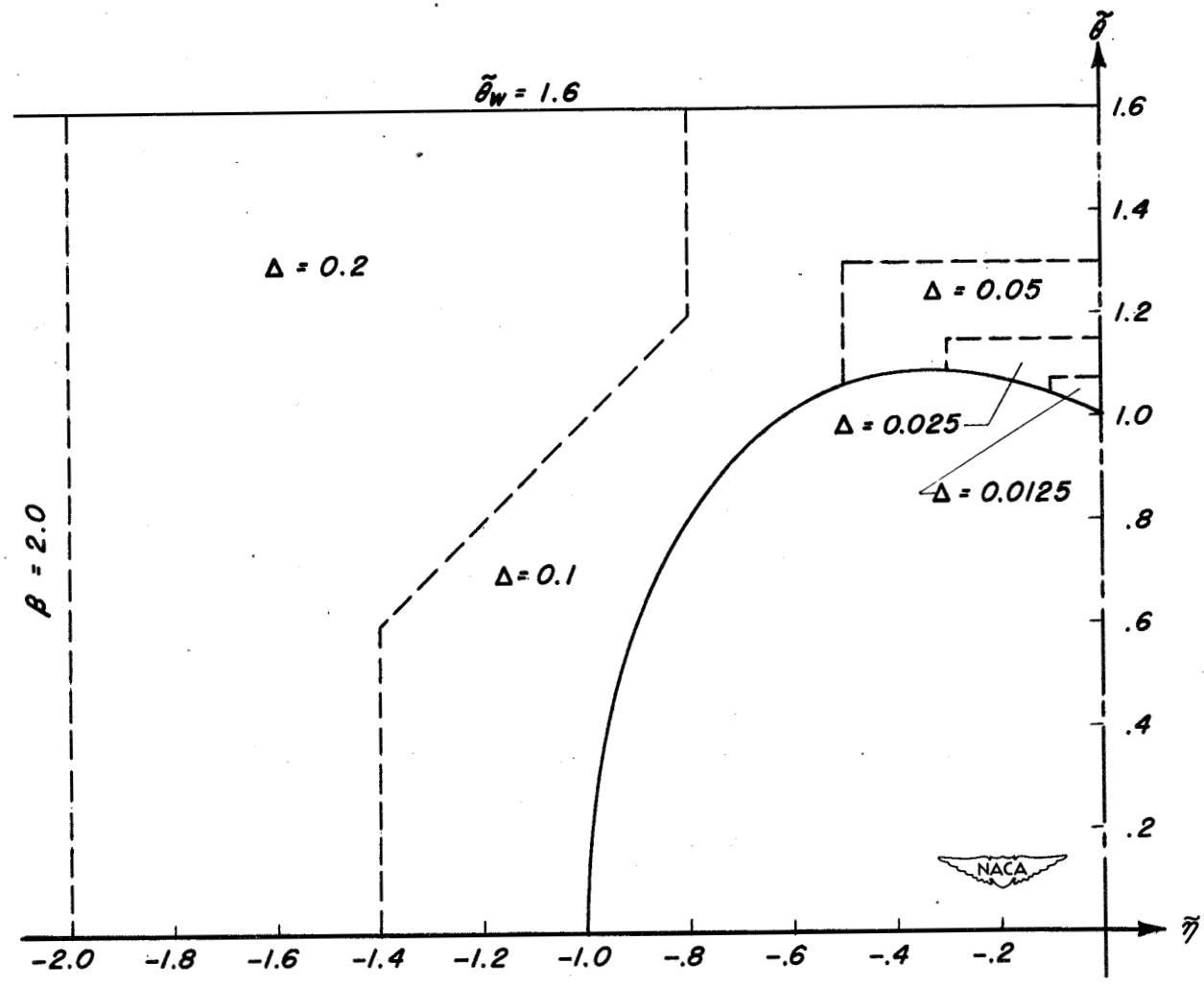

Figure 2.– Distribution of lattice spacing for $\tilde{\theta}_w = 1.6$.

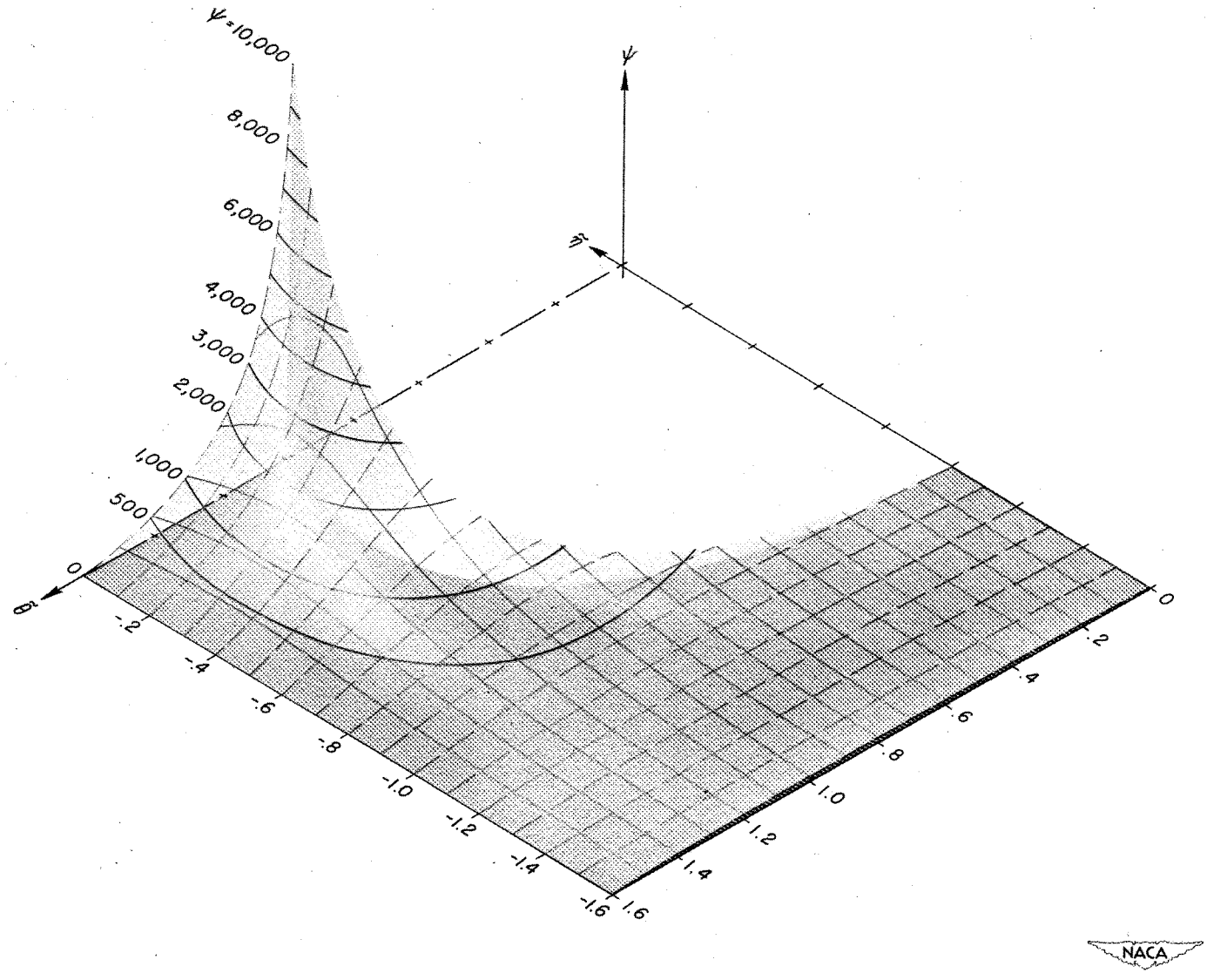

Figure 3.- Representation of $\tilde{\psi}$ as a function of $\tilde{\eta}$ and $\tilde{\theta}$ for $\tilde{\theta}_w = 1.6$ ($\xi_o = 0.921$).

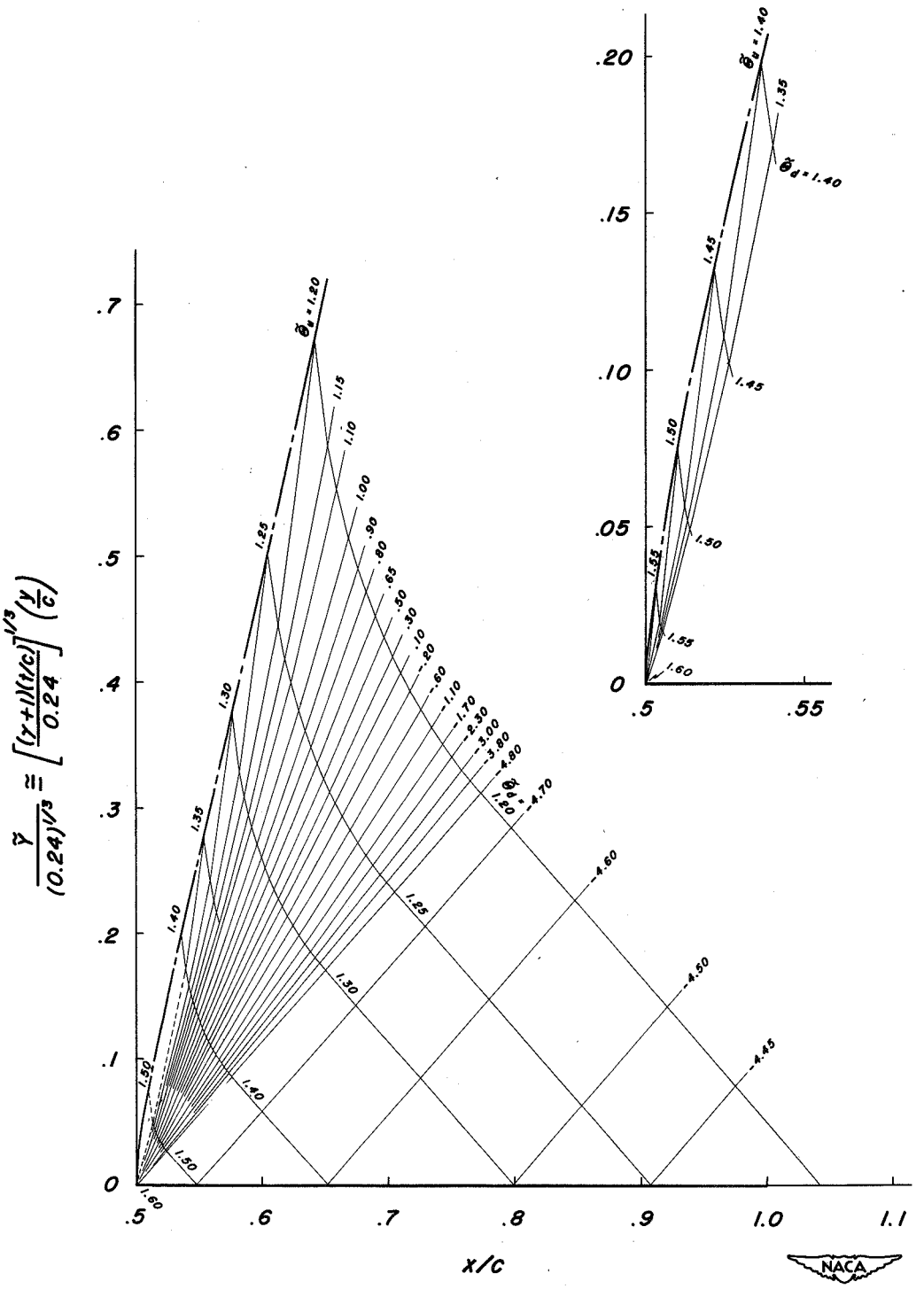

Figure 4.- Mach net over rear of airfoil for $\tilde{\theta}_w = 1.6$ ($\xi_o = 0.921$).

NACA TN 2588
National Advisory Committee for Aeronautics.
TRANSONIC FLOW PAST A WEDGE PROFILE WITH DETACHED BOW WAVE - DETAILS OF ANALYSIS.
Walter G. Vincenti and Cleo B. Wagoner. December 1951. 48p. diagrs., tab. (NACA TN 2588)

Details are given of the calculations of the flow with detached bow wave past a doubly symmetrical, double-wedge profile at zero angle of attack. The results of these calculations have been previously described in NACA TN 2339.

Copies obtainable from NACA, Washington

1. Flow, Mixed (1.1.2.2)
2. Wing Section Theory (1.2.1.1)
3. Research Technique, Mathematics (9.2.7)

I. Vincenti, Walter G.
II. Wagoner, Cleo B.
III. NACA TN 2588

NACA TN 2588
National Advisory Committee for Aeronautics.
TRANSONIC FLOW PAST A WEDGE PROFILE WITH DETACHED BOW WAVE - DETAILS OF ANALYSIS.
Walter G. Vincenti and Cleo B. Wagoner. December 1951. 48p. diagrs., tab. (NACA TN 2588)

Details are given of the calculations of the flow with detached bow wave past a doubly symmetrical, double-wedge profile at zero angle of attack. The results of these calculations have been previously described in NACA TN 2339.

Copies obtainable from NACA, Washington

1. Flow, Mixed (1.1.2.2)
2. Wing Section Theory (1.2.1.1)
3. Research Technique, Mathematics (9.2.7)

I. Vincenti, Walter G.
II. Wagoner, Cleo B.
III. NACA TN 2588

NACA TN 2588
National Advisory Committee for Aeronautics.
TRANSONIC FLOW PAST A WEDGE PROFILE WITH DETACHED BOW WAVE - DETAILS OF ANALYSIS.
Walter G. Vincenti and Cleo B. Wagoner. December 1951. 48p. diagrs., tab. (NACA TN 2588)

Details are given of the calculations of the flow with detached bow wave past a doubly symmetrical, double-wedge profile at zero angle of attack. The results of these calculations have been previously described in NACA TN 2339.

Copies obtainable from NACA, Washington

1. Flow, Mixed (1.1.2.2)
2. Wing Section Theory (1.2.1.1)
3. Research Technique, Mathematics (9.2.7)

I. Vincenti, Walter G.
II. Wagoner, Cleo B.
III. NACA TN 2588

NACA TN 2588
National Advisory Committee for Aeronautics.
TRANSONIC FLOW PAST A WEDGE PROFILE WITH DETACHED BOW WAVE - DETAILS OF ANALYSIS.
Walter G. Vincenti and Cleo B. Wagoner. December 1951. 48p. diagrs., tab. (NACA TN 2588)

Details are given of the calculations of the flow with detached bow wave past a doubly symmetrical, double-wedge profile at zero angle of attack. The results of these calculations have been previously described in NACA TN 2339.

Copies obtainable from NACA, Washington

1. Flow, Mixed (1.1.2.2)
2. Wing Section Theory (1.2.1.1)
3. Research Technique, Mathematics (9.2.7)

I. Vincenti, Walter G.
II. Wagoner, Cleo B.
III. NACA TN 2588